# Master Thesis

진동형 히트파이프에 대한 실험 및 이론적 연구

## An Experimental and Analytical Study on Pulsating Heat Pipe

**Supervisor: Professor Kwang-Hyun Bang**

**January 2019**


**Graduate School of Korea Maritime and Ocean University**

Department of Refrigeration and Air-Conditioning Engineering

**VO DUY TAN**

# Master Thesis

진동형 히트파이프에 대한 실험 및 이론적 연구

## An Experimental and Analytical Study on Pulsating Heat Pipe

**Supervisor:**

**Professor Kwang-Hyun Bang**

by

**Vo Duy Tan**

A thesis submitted in partial fulfillment

of the requirements for the degree of

**Master of Science in Refrigeration and Air-Conditioning Engineering**

Graduate School of Korea Maritime and Ocean University

**January 2019**

본논문을 **VO DUY TAN**의 공학석사 학위논문으로 인준함.

위원장: 공학박사 박권하 **(**인**)**

위 원: 공학박사 도덕희 **(**인**)**

위 원: 공학박사 방광현 **(**인**)**

**2018** 년 **12** 월 **19** 일

한국해양대학교 대학원

# An Experimental and Analytical Study on Pulsating Heat Pipe

Vo Duy Tan

Department of Refrigeration and Air-Conditioning Engineering
Graduate School of Korea Maritime and Ocean University

## Abstract

With the rapid development of the semiconductor material technology, the operating power of processors has the trend to increase higher. The pulsating heat pipe (PHP) or oscillating heat pipe with the high performance and simple structure is a promising heat transfer device for a lot of applications in further technology.

In the present study, a three-dimensional closed-loop pulsating heat pipe has been simulated and compared with the experiment. The present study concentrates on analyzing and predicting the behavior of motion of fluid flow inside the pulsating heat pipe. A model of pulsating heat pipe with eight-turn was fabricated using Pyrex tubes with the inner diameter of 1.85 mm. The boundary temperatures for the evaporator and condenser were 80ºC and 25ºC. For working fluid, R123 was employed in this study because of its sensibility characteristic on the motion. The charging ratios were 50% and 60%. Flow visualization through the transparent chambers using a high-speed camera was recorded to study the flow motion. The circulation motion was observed in both experiment and simulation.

The simulation results of the motion characteristics showed a good agreement with the experimental data. The simulation results of flow pattern, heat transfer rate, and pressure were also discussed. The results have been analyzed to understand better about the mechanism of PHP and they provided lessons for progressing to further modeling.

# List of Contents

# List of Tables

# List of Figures

# Nomenclature

| Symbols | Description |
|---|---|
| t | time (s) |
| $m_{lv}$ | mass evaporated ($kg/s/m^3$) |
| $m_{vl}$ | mass condensed ($kg/s/m^3$) |
| $F$ | force |
| T | temperature (K) |
| $r_l$ | relaxation time |
| $u$ | velocity vector (m/s) |
| P | pressure (Pa) |
| $g$ | gravity ($m/s^2$) |
| $F_{CSF}$ | continuum surface force (N) |
| $C_v$ | surface curvative |
| $E$ | energy (J) |
| $S_E$ | energy source term ($W/m^3$) |
| Bo | Bond number |
| Eo | Eotvos number |
| D | diameter (m) |
| Q | heat transfer rate (W) |
| $C_p$ | specific heat capacity (J/K kg) |

Greek letters

| | |
|---|---|
| θ | inclination angle |
| σ | surface tension (N/m) |
| ρ | density (kg/m3) |
| α | void fraction |
| $k$ | thermal conductivity (W/ m. K) |
| τ | shear stress (N/m$^2$) |
| $\mu$ | dynamic viscosity (Pa. s) |
| $h$ | heat transfer coefficient (W/m$^2$.K) |

Subscripts

| | |
|---|---|
| l | liquid |
| v | vapor |
| f | fluid |
| SAT | saturation state |

# Chapter 1 Introduction

## 1.1 Fundamental definition of PHP

The early study of Pulsating Heat Pipe (PHP) was presented in the 1990s by Akachi [1]. Fundamentally, PHP is a type of heat pipe with the body bent as shown in Fig. 1. The geometry of PHP is simple and could be divided into two types: open-loop and closed-loop PHP. The geometry of them can be examined in Fig. 1.

Like the conventional type of heat pipes, the PHP should be degassed before charging the working fluid. The charging ratio of fluid normally varies from 20 to 80 percent for higher performance, depending on the type of working fluid. After charging, the liquid slug and vapor plug distribute randomly inside the tube. Normally, the PHP is divided into three zones: heating, adiabatic and cooling section as shown in Fig. 1. When the system operates, because the expansion and collapse of the vapor plug at the heating section and cooling section respectively, the pressure of each section becomes different and the oscillating motion occurs. Because the travel of fluid, the heat will be transported from the evaporator section to the condenser section.

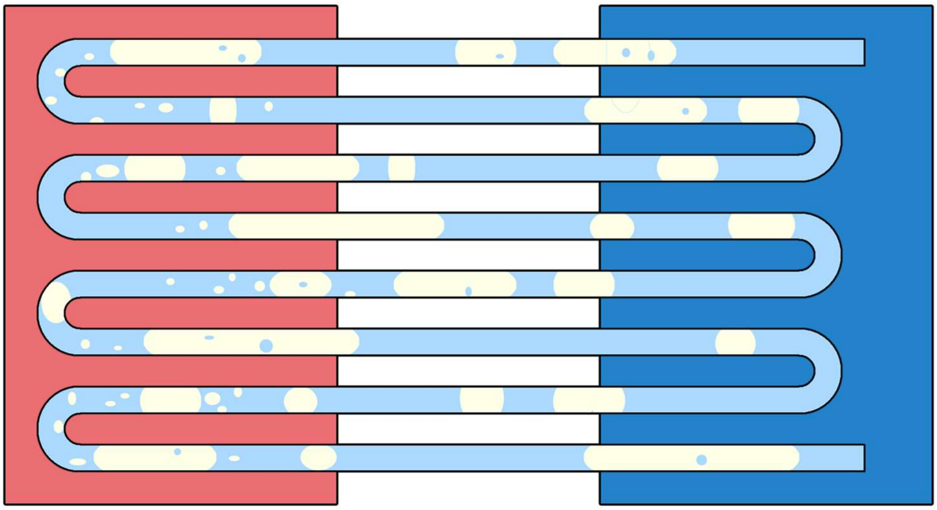

(a) Open-loop PHP

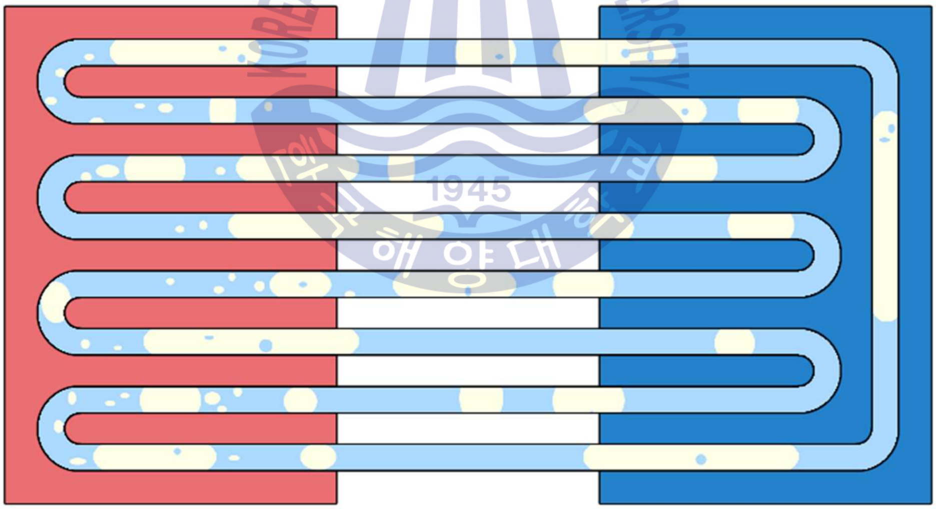

(b) Closed-loop PHP

Figure 1. Illustration of PHP: (a) Open loop and (b) Closed loop PHP

## 1.2 Applications of PHP

Many applications of PHP have been invented such as solar energy utilization, waste heat recovery, aerospace thermal management and electron cooling due to its distinct advantages:

(1) Simple structure and low cost: PHP is made of a long capillary tube, which is bent into many turns. The characteristic that no wick structures are required. The small diameter of the PHP is also helpful for cost saving;

(2) Excellent heat transfer capability: the equivalent thermal conductivity of PHP can be as high as dozen times of that of copper;

(3) Easy to realize miniaturization: the size of the PHP heat transfer device can be very small due to the small inner diameter of the PHP, which is one of the most attractive characteristics of the PHP;

(4) High flexibility: the channel of PHP can be arranged to arbitrary configuration according to the condition of application.

PHP is a proven simple, reliable and an economically feasible choice for heat transfer. Although the structure of a PHP is quite simple, the coupling of hydrodynamic and thermodynamic effect during the process of heat and mass transfer in PHP makes the operational mechanism of PHP very complicated and hard to be fully revealed. Because of this extensive investigation of the behavior of motion is necessary.

In the present study, experiment and simulation were performed to study the mechanism of PHP with the working fluid of R123. The objective of this study is to analyze the motion behavior to understand better about the operating PHP. Furthermore, this study can be applied to the micro PHP that has promising potential.

# Chapter 2 Literature Review

## 2.1 Experimental work

After over two decades of investigation and development, many types of research have performed to get the best understanding of the behavior of the PHP. Groll and his partners have vastly contributed to the apprehending mechanism of PHP [2-4]. Their research considered wide range of factors, which effect on the operating mechanism of PHP, including the type of working fluid, internal diameter, charging ratio, the number of channels and the supplied power. The effect of the other parameters on the operation of PHP was summarized and presented on the review paper [5-6].

The heat transfer performance of the PHP is greatly influenced by the various parameters, which can be divided into three groups:

(1) Geometric parameters of PHP: such as the inner diameter, the cross-section shape of the PHP, channel configuration, the length of the evaporation and condensation section, the number of turns, etc.;

(2) Physical properties of working fluid: the thermodynamic and the hydrodynamic properties of the working fluid, such as surface tension, latent heat, viscosity, etc.; and

(3) Operational parameters: charge ratio, heat flux, inclination angle, external force, etc.

### 2.1.1 Influence of geometric parameters

#### A. Inner diameter

The inner diameter is a parameter which closely relates to the definition of the PHP. The normal operation of PHP is based on the oscillation motions of vapor slugs and liquid plugs and whether the vapor slugs and liquid plugs can be formed in the PHP depends on the relative strength of the gravity and surface tension, as indicated by the Bond number

$$Bo = \sqrt{Eo} = \sqrt{\frac{g(\rho_l - \rho_g)}{\sigma} D^2} \tag{1}$$

Frictional resistance increases with the decrease of inner diameter when the inner diameter is very small. The inner diameter of the PHP is normally suggested to be within the following range [7]:

$$0.7\sqrt{\frac{\sigma}{g(\rho_l - \rho_g)}} \leq D \leq 2\sqrt{\frac{\sigma}{g(\rho_l - \rho_g)}} \tag{2}$$

In addition, the inner diameter also has a significant influence on the heat transfer performance of the PHP, which has been extensively investigated. Yang et al. [8] concluded that the PHP with larger inner diameter showed better thermal performance than that of smaller one, and it was attributed to lower dissipative losses when the inner diameter of PHP was larger. Charoensawan et al. [9] found that at each evaporation temperature, the thermal resistance of the PHP was distinctly reduced with the increase of the inner diameter. This was because that the smaller inner diameter led to larger frictional resistance. Besides, it should be noted that the physical properties of working fluid might have an influence on the effect of inner diameter on the performance of PHP as indicated by Rittidech et al. [10]. It was found that larger the inner diameter, the better heat transfer performance for the R123 while the worse for ethanol. From the contents above, it could be seen that the inner diameter has a great impact on the heat transfer performance of PHP. When the inner diameter of PHP is small, the frictional resistance of the working fluid is large, and greater heat flux is needed to maintain the oscillation motions of the working fluid. Meanwhile, the impact may be coupled with other parameters, such as the charge ratio and the properties of the working fluid.

### B. Number of turns

Because of the unique flow characteristics of the working fluid in U-turns, the pressure losses are more considerable than that in the straight tube, and the secondary flow is more likely to occur. The number of turns significantly influences the internal pressure distribution and the heat transfer characteristics of the PHP. Quan et al. [11] proposed that the increasing number of turns could improve the internal pressure disturbance and obtain a better heat transfer performance of the PHP. Yang et al. [12] developed a PHP consisted of 40 parallel channels, it was found that the PHP operated successfully with all inclination angles. As a key point, researches [3,14] pointed out that there existed a critical number of turns to make the performance of PHP independent of the inclination angles when the actual number of the turns was greater than it. According to the work of Charoensawan et al. [2], the critical number of turns of the PHP was influenced by the properties of working fluid and the inner diameter of the tube.

Until now, it is still unclear how to theoretically analyze and obtain the critical number of turns and how the critical number of turns is influenced by the other parameters.

### 2.1.2 Influence of physical properties of working fluid

Among the numerous methods to improve the heat transfer performance of PHP, the most direct and effective one is to select an excellent functional fluid as the working fluid. The physical properties of the working fluid, such as the surface tension and wettability, latent heat, specific heat, viscosity have profound effects on the heat transfer performance of PHP.

#### A. Surface tension

The static contact angle of the working fluid on tube wall is a constant value and can be calculated, while the dynamic contact angle depends on the characteristics of oscillation of the working fluid. The dynamic contact angle changes within a range when the working fluid is oscillating in the pipe, so the oscillation motions of the working fluid will be affected by the capillary resistance.

On the one hand, the capillary resistance is in proportion to the surface tension. Larger surface tension causes larger capillary resistance. On the other hand, the working fluid with higher surface tension will increase the critical diameter of the PHP according to Eq. (1), leading to the enlargement of the allowed extent of the inner diameter for PHP and relative better performance of PHP because of lower frictional resistance when the inner diameter is larger [14]. The actual influence of the surface tension on the heat transfer performance of PHP is the tradeoff of these two aspects.

B. Latent heat

Lower latent heat will be beneficial to help the bubbles generating and condensing more quickly, as well as shorten the startup time of the PHP. When the latent heat of the working fluid is low, lower superheat of tube wall can start the PHP [5]. So, it is suggested that when the heat flux is very low, the working fluid with lower latent heat is desirable. However, when the heat flux is very high, the latent heat becomes the dominant part of the heat transfer process, so the working fluid with higher latent heat can dissipate more heat from the evaporation section.

C. Specific heat

When the heat flux input to the evaporation section is very low, most of the heat is dissipated by the sensible heat. The specific heat also closely relates to the heat capacity of working fluid [14].

D. Viscosity

It is easy to understand that the working fluid with a lower viscosity is a better choice for the PHP. A low dynamic viscosity will reduce the shear stresses in the channel and decrease the pressure losses. This will reduce the required heat flux to maintain the oscillation motion [15].

E. Thermal conductivity

The effect of thermal conductivity of the working fluid on PHP is not only reflected on the temperature distribution but also the response time of PHP. Larger the thermal conductivity is, faster the heat can transfer in the PHP. Furthermore, it can also decrease the temperature difference between the evaporation section and the condensation section.

Experimental studies were carried out to investigate the heat transfer performance of PHP with different working fluids. Qu et al. [7] carried out a visualization study with three silicon-based micro PHPs. It was found that when the PHPs were charged with R113 and FC-72, they could start up successfully, but when the working fluids were water and ethanol, they failed to start up at all inclination angles. Charoensawan et al. [2] claimed that when the inclination angle of the PHP was 90º (the condensation section of the PHP is above the evaporation section), the PHP with water showed better performance when compared with R123 and ethanol. Qu et al. [16] presented an experimental investigation of the heat transfer performance of a micro-PHP. The results suggested that R113 was suitable for the micro-PHP at lower heat flux, while FC-72 was more favorable when the heat flux was higher.

F. Nanofluid:

Using nanofluid as a working fluid in a thermal management device is one of the hot research topics in heat transfer enhancement area due to their excellent properties. The nanofluid is a homogeneous, stable mixture which includes a base fluid and nanoparticles, which are used to enhance the heat transfer process. Recently, nanofluids have been used as a working fluid to improve the heat transfer performance of PHP. Qu et al. [17] proposed that when the nanofluid was used as the working fluid, the PHP could startup quickly and operate stably at lower heat flux. At the same time, the thermal resistance of the PHP with $TiO_2/H_2O$ nanofluid was lower than that of PHP with water. In the experimental investigation of Lin et al. [18], the working fluids included the $Ag/H_2O$ nanofluid and water. It was observed that both the average temperature difference and the thermal resistance of PHP were decreased significantly when the working fluid was silver nanofluid, compared with the water. Meanwhile, it was suggested that the nanoparticle's settlement in the evaporation section was the major reason for the enhancement of the heat transfer process.

The influence of the working fluid on the PHP is the tradeoff result of these physical properties. Using nanofluid as the working fluid is an effective method to improve the heat transfer performance of the PHP, while the effect depends on the concentrations of the nanoparticles [19, 20]. It seems that the effect of enhancement is obvious when the concentration is very low, but the heat transfer performance of the PHP may deteriorate when the concentration significantly increases.

### 2.1.3 Influence of operational parameters

#### A. Charge ratio

Charge ratio is defined as the ratio of working fluid volume to the total volume of the PHP. Because the relative number of liquid plugs and vapor slugs depends on the charge ratio, the charge ratio has a significant influence on the performance of PHP. If the charge ratio is too low, there are too many vapor slugs in the PHP and it is very hard to sustain the stable vibration; on the other hand, the heating capacity of the PHP is also limited, and the phenomenon of dry-out occurs easily. If the charge ratio is too high, there are few vapor slugs in the pipe, which causes the driving force of the working fluid decreasing and the operation of PHP will be very difficult. When the charge ratio equals to one, the PHP would become a tube full of working fluid, in which case only sensible heat transfer of the working fluid and tube wall could be applied to dissipate the heat. Experimental studies have shown that when the charge ratio is between

0.2 and 0.8, the PHP can operate normally [21]. However, there exists an optimal range of the charge ratio for PHP, in which the PHP shows better performance than that beyond this range. When the charge ratio of the PHP is in the optimal range, the fluctuation of pressure can promote the oscillation motions of working fluid efficiently, and the liquid plugs can dissipate enough heat from the evaporation section to the condensation section at the same time.

Some researchers have reported the existence of the optimal charge ratio. Qu et al. [22] investigated the influence of working fluid on the optimal charge ratio for an embedded flat PHP. The results showed that for PHP with acetone and FC-72, the optimal charge ratio was 0.36 and 0.67, respectively. Yang et al. [8] investigated the heat transfer performance of PHP with ethanol and it was pointed out that the optimal range of charge ratio was 0.50–0.65 when the inclination angle of the PHP was 0° or 90°.

In general, the optimal charge ratios proposed by above mentioned researches were usually suitable for the PHP operated in the test conditions. It seems that the optimal charge ratio of PHP varies with the different combination of other parameters, such as the working fluid, the inclination angle and the heat flux.

B. Inclination angle and gravity

If the inner diameter of a PHP satisfies Eq. (3), the impact of the surface tension of the working fluid will be stronger than the gravity. However, the gravity still has a significant influence on the heat transfer performance of PHP [23]. The research methods utilized to investigate the influence of gravity can be classified into two groups: one is by changing the inclination angle of the PHP and the other is by changing the gravity field. When the inclination angle is changing, the influence of the inclination angle on the heat transfer performance of the PHP is obvious. The PHP with the inclination angle of 90º showed better performance than the PHP with another inclination angle. Under this condition, the gravity helped the working fluid to oscillate in the PHP. Nevertheless, the following researches indicated that this conclusion might not suit for the PHP with special geometric structures. Vassilev et al. [21] investigated the influence of the inclination angle using a flat plate PHP. The results indicated that the thermal resistance of the PHP slightly increased with the inclination angle when it was within the range of 0–90º.

The influence of inclination angle and the gravity on the heat transfer performance of PHP is very complex, and it is highly coupled with a specific type and the operational conditions of the PHP.

### C. Heat flux

The input heat flux is also an important parameter for the heat transfer performance of the PHP. The influence of the heat flux on PHP has mainly embodied in two aspects: the startup heat flux of the PHP and the relationship between the heat flux and the heat transfer performance of PHP. For the first aspect, the experimental results [9] indicated that there existed a minimum heat flux to make the PHP start to operate and only when the input heat flux was greater than this minimum value that the PHP can operate successfully. Otherwise, no apparent oscillation motions of the working fluid can be observed. This minimum heat flux is usually called the startup heat flux of the PHP.

For the second aspect, it is the pressure difference caused by the input heat flux that drives the working fluid to oscillate in the PHP, so the heat flux has a close relationship with the characteristics of the oscillation motions, as well as the heat transfer performance of the PHP. In addition, the heat flux also affected the ratio of the sensible heat to the latent heat during the process of heat transfer. When the heat flux is very low, the sensible heat will dominate the heat transfer process and the latent heat takes up when the heat flux becomes higher [5]. The thermal resistance of the PHP decreases with the increase of heat flux [18].

Basically, the oscillation motions of the working fluid in a PHP have unique characteristics and closely related to the heat flux. When the heat flux is very low but enough to start the PHP, the dominant flow pattern of the working fluid is the slug flow. Under this condition, the oscillation of the working fluid is quite random with very low velocity. As the heat flux becomes higher, the flow pattern will change to semi-annular flow and even the annular flow [5]. In this case, the oscillation motions of working fluid become very violent with high flow velocity, and more heat is dissipated.

Wilson et al. [24] investigated the oscillation motions of the PHP by the neutron radiography technology. It was pointed out that the oscillation direction of the working fluid was random when the heat flux was very low.

Characterization of fluid motion was investigated on the visualization research [36-38]. The motion with the directional circulation was observed in the flow visualization experiment of Tong [25]. The research also indicates the influences of the meandering bend, even slug, and plug distribution and non-concurrent boiling on the oscillation and circulation phenomena of the PHP. The study of Khandekar indicates the relative between the variations of supplied power with the motion regime. Especially, the regime of motion change from oscillation regime to circulation regime with the increasing of power [25]. The study of Zhi Hu Xue denotes that the thermo-hydrodynamic characteristics and thermal performance have a direct relationship with the distribution of vapor bubbles and liquid slugs which are called the flow patterns in the tubes [26]. The breakup and recombine process of a liquid slug at the bend was also presented and analyzed on their investigation. The investigations above have brought the largely progressing on the cognition of PHP. Although that the motion behavior and the difference between circulation and oscillation regime of PHP still be indistinct and need a definition.

## 2.2 Analytical work

To understand the operating mechanism of PHP, some researchers have investigated and developed the numerical model, empirical correlations or have used a commercial CFD program. Shafii presented analytical models of thermal behavior and heat transfer of the PHP base on the one-dimensional model [27]. Following that many mathematical models have been investigated to analysis the complicated behaviors of motion mechanism [28-30]. Bae investigated the effect of film dynamics on fluid motion and thermal performance in PHP [31]. The results show the success in predicting thermal performance, compared with experimental data, not only for a vertical PHP but also for horizontal and inclined PHP with various different parameters.

In the CFD field, with the development of the computer, several types of research used the commercial program like CFX and Fluent to simulate the PHPs. A two-dimensional simulation based on the volume of fluid (VOF) and mixture model was presented by Zirong Lin [32]. The research showed that the mixture model was more suitable for the two-phase flow simulation in a PHPs. S.M. Pouryoussefi also conducted two-dimensional simulation, which analyzes the chaotic flow behavior for 2 turns and multi-turn CPHP [33]. VOF method has been employed in their simulation. The formation of perfect vapor, liquid plugs, and the liquid film was observed in their study. It also leads out by increasing the charging ratio and evaporator heating power the correlation dimension increases [33].

A flat-plate oscillating heat pipe (FP-OHP) was simulated using a three-dimensional model [34]. The study pointed out that the generation and characteristic of vapor slugs and liquid plugs come from the self-growth and coalescence of dispersed bubbles. Generally, the above study was led better understanding of the mechanism. However, the researches above still not completely successful in predicting the motion behavior of PHP. And the effect of pressure on the motion still not reveal and appropriately concern.

Therefore, in the current study, a three-dimension numerical investigation was conducted to predict the motion of fluid flow with the variation of charging ratio. The numerical simulation was performed in parallel with the experiment to compare and evaluate better. The visualization of fluid flow was recorded by the high-speed camera to investigate on the motion of fluid flow. Moreover, thermal performance, flow pattern, wall temperature, and the pressure distribution along the length of the tube were also processed in this study.

# Chapter 3 Experiment

## 3.1 Introduction

The test section was designed to observe the motion of fluid flow. The PHP was fabricated by using Pyrex tubes of 3.02 mm of the outer diameter and 1.85 mm of inner diameter. Sixteen tubes were equally spaced by 26.15 mm. Experiments were conducted for a vertical orientation with a bottom heating mode.

Figure 2 (a) and (b) illustrate the photograph and drawing of the design modeling. A high-speed camera was used to visualize the flow behaviors inside the PHP. R123 was used in this study because of its fast vaporizing characteristic.

## 3.2 Experimental apparatus

### 3.2.1 Experimental apparatus and procedure

The list of experimental parameters is presented in Table 1. The schematic of the experimental setup is given in Figure 3. The system was designed with two 3-valves installed on the adiabatic 1 for degassing and charging process. The PHP was evacuated to less than 0.3 kPa by using the vacuum pump. The degassing process maintained at least 4 hours to assure the pipe was totally evacuated. After that, the working fluid is charged into the PHP. After evacuating and charging process, the constant-temperature bath circulations turn on and circulates the heating and cooling water through the water chambers. The water flow rate was maintained at 1 LPM using the flow meter. The heating and cooling water were maintained at 80°C and 25°C, respectively. The temperature data was recorded from the time the system starts to operate until the system stops operation, and the visualization is recorded for the period of steady state of the system. The list of devices is shown in Table 2.

The procedure includes 5 steps:

(1) Degassing process;

(2) Charging process;

(3) Supply cooling and heating water into water chambers;

(4) Recording data and videos;

(5) Turn off the system.

Table 1. Experimental parameters

| Parameter | Value |
|---|---|
| Diameter | 1.85 mm |
| Channel | 16 channels (8 turns) |
| Operating Mode | Vertical (bottom heat) |
| Temperature:<br>- Heating<br>- Cooling | <br>80°C<br>25°C |
| Working fluids | R123 |
| Charging ratio | 50 - 60% |
| Water flow rate | 1 LPM |

Table 2. List of main devices

| Main devices | Purpose | Picture |
|---|---|---|
| High-speed camera:<br>. Photron FAST-CAM SA4 | Record the video |  |
| Data acquisition system<br>. National instruments Ni SCX1 1000 | Record the temperature data |  |
| Bath circulation<br>. RW-0525G Jeio tech | Supply cooling and heating water. |  |
| Laptop | Store and process data |  |
| Pressure gauge | Measure the vacuum condition. |  |

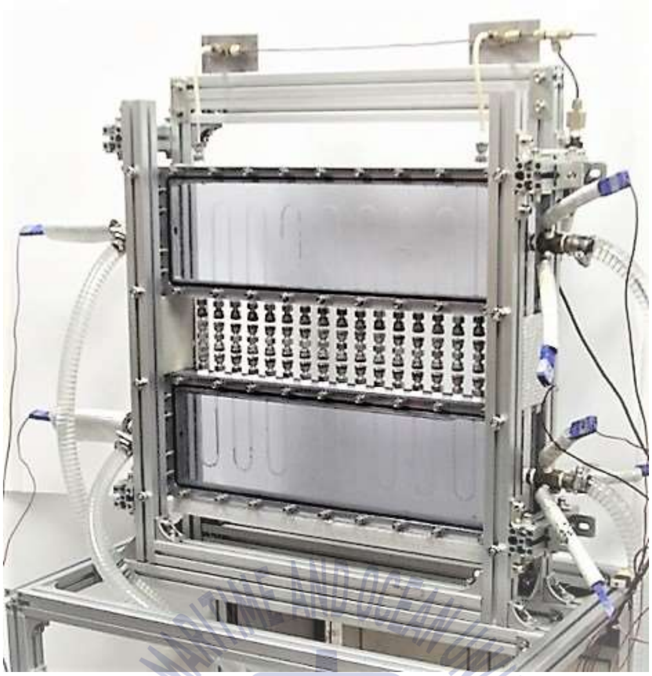

(a)

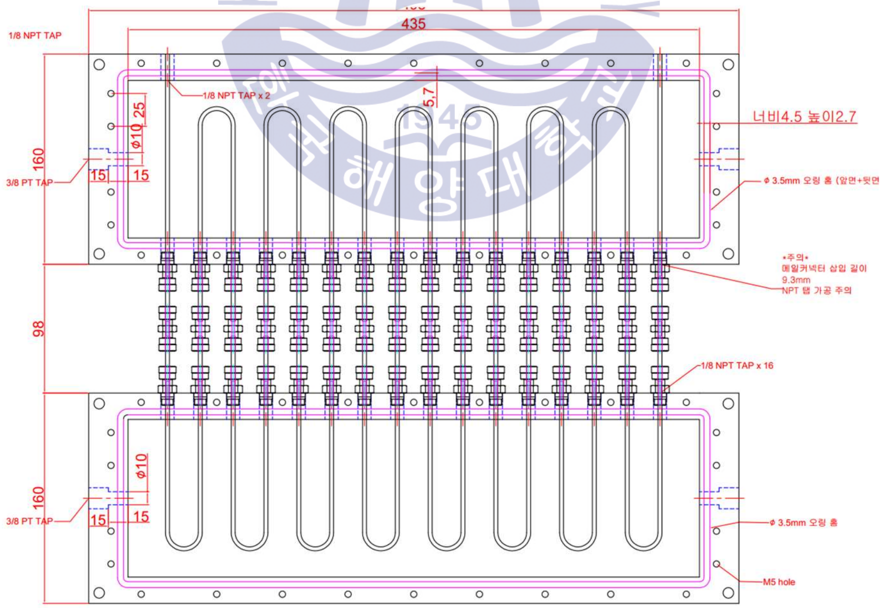


(b)

Figure 2. (a) Photograph and (b) schematic of PHP

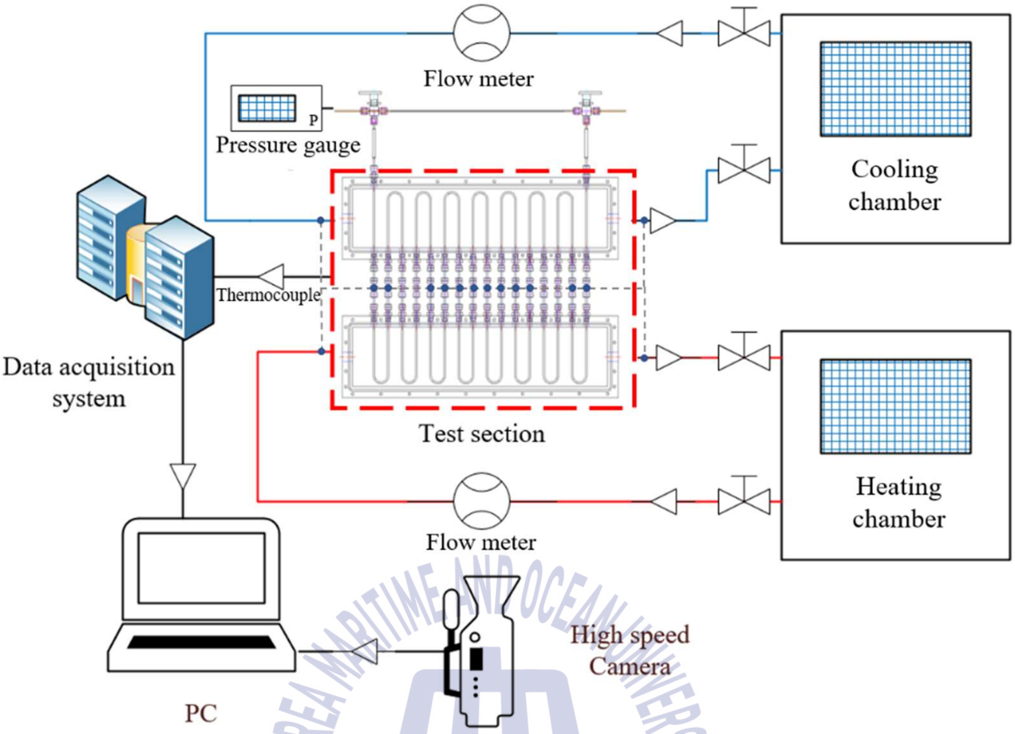


Figure 3. Schematic diagram of experimental apparatus

### 3.2.2 Measurement

Temperature values were measured using T-type thermocouples at 12 points attached on the Pyrex wall and 4 points at the inlet and outlet ports of the heating and cooling chambers. The positions of the thermocouples are given in Figure 4.

The heat transfer rate was calculated using the inlet and outlet temperature values of water chambers.

$$Q = m \times C_p \times |(T_{out} - T_{in})| \tag{3}$$

The fluid motion was recorded using a high-speed camera. The videos were recorded at a steady-state time. The visual results were recorded in the area: total, bottom-center, and top-center view.

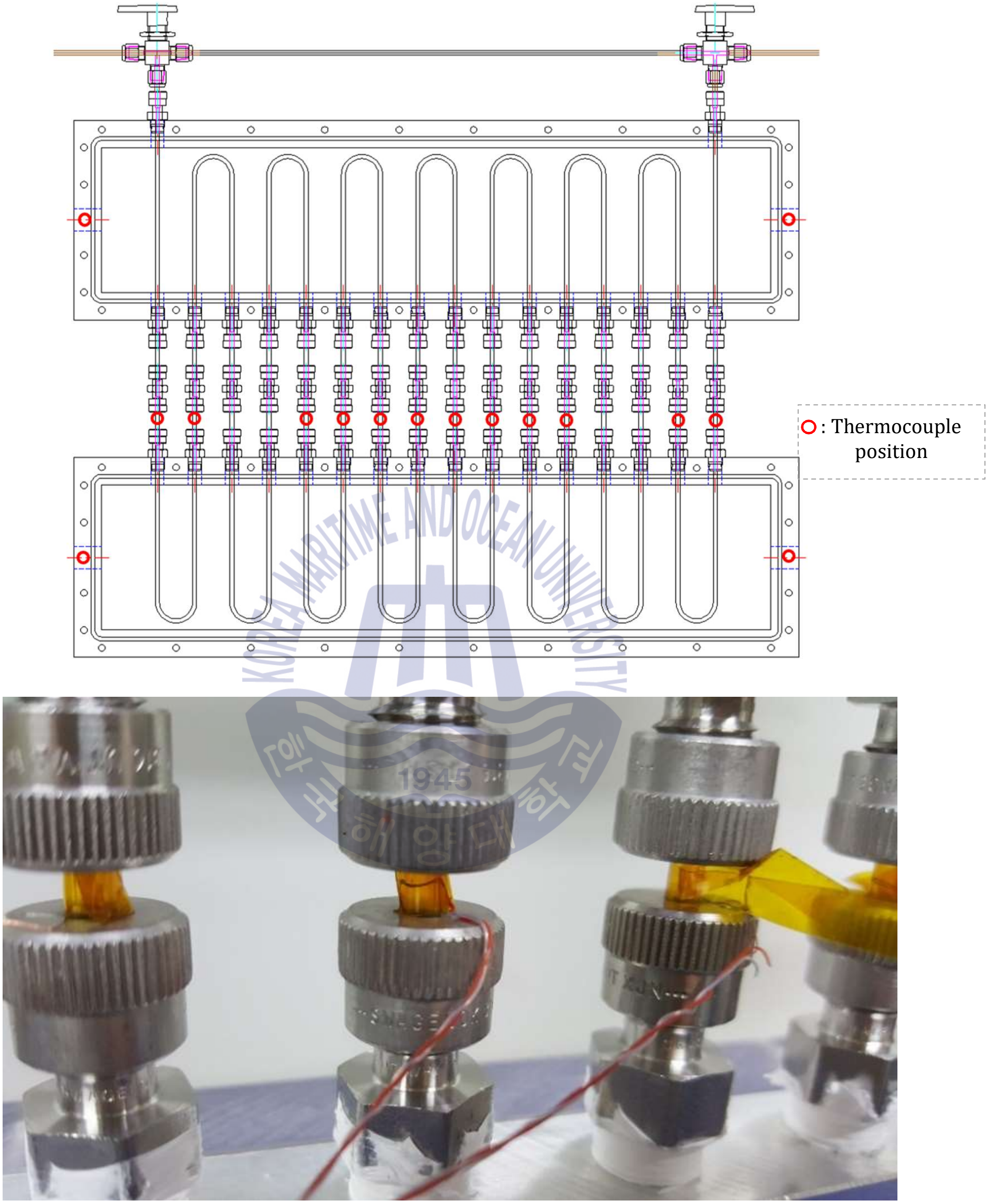


Figure 4. Locations of thermocouple attachment

## 3.3 Results and discussions

### 3.3.1 Visual observation of flow patterns

When a boiling process takes place, a variety of configurations known as flow patterns were observed. The particular flow pattern depends on the condition of pressure, flow, heat flux, and channel geometry. Each has a descriptive name and it is desirable to identify what the flow pattern or successive flow patterns are so that a hydrodynamic or heat transfer which is theory appropriate to that flow pattern can be chosen. Figure 5 and 6 show the flow pattern at the heating and cooling sections.

The results showed that the churn and slug flows were normally observed in the top cooling section. It could be explained from the difference of velocities between the liquid slug and vapor plug. On the top section, because the condensation process occurs, the velocity of liquid slug and vapor plug are low. And the feature of this moving represents the churn and slug slow.

Figure 6 shows the flow pattern of fluid flow at the bottom section. The bubbly flow was observed. The explanation is the moving with a high velocity of the dispersed bubble which was caused by the boiling of fluid flow at the bottom section. The evaporation of fluid flow occurs violently in this case because R123 has low latent heat. Thus, the evaporation process will be fast and flexible.

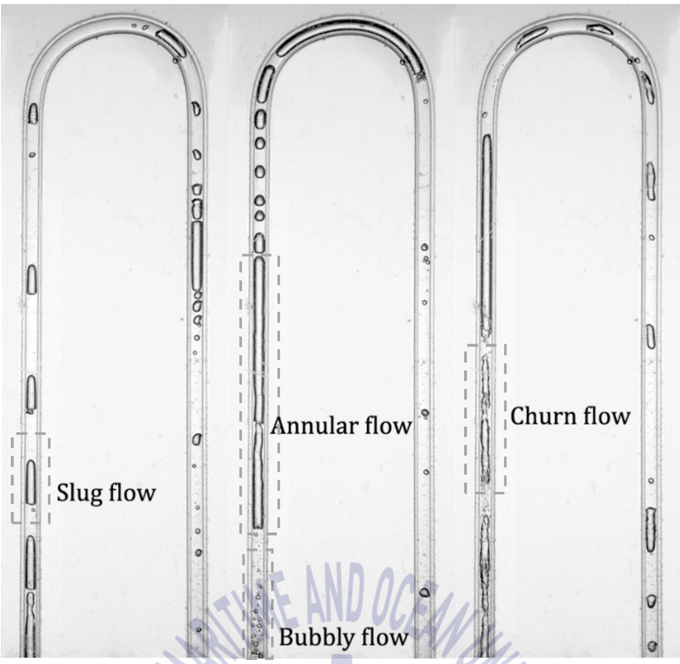


Figure 5. Flow pattern of fluid flow at the cooling section

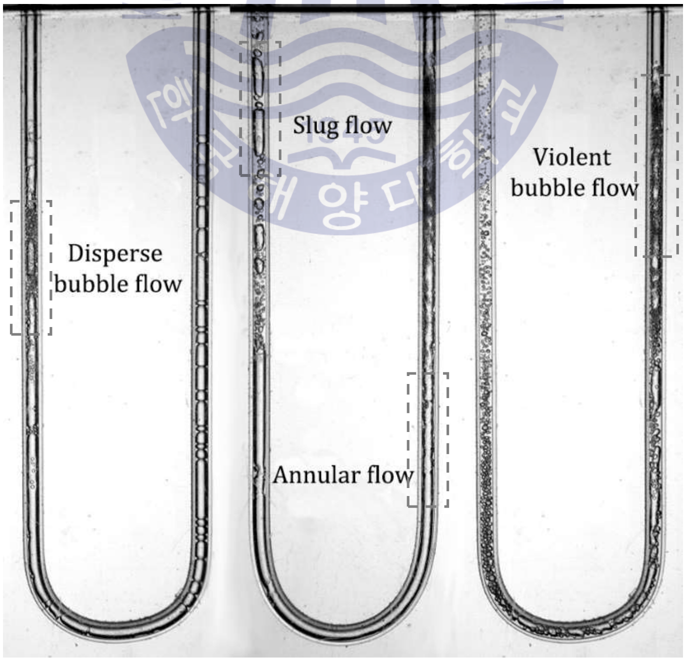


Figure 6. Flow pattern of fluid flow at the heating section

### 3.3.2 Heat transfer rate

The heat transfer rate was calculated using the equation (3) for the steady-state time of the system. The results were summarized in Table 3. It showed that the operation of open-loop PHP was unstable. In particular condition, the open-loop case did not work. The reason was due to the geometry of the open-loop PHP and the liquid-vapor distribution. In particular condition, if most of liquid slugs locate in the left or right side of the pipe then the device will not work. This problem could be self-solved in the case of closed-loop PHP. The results showed that closed-loop PHP operated stably in all case. It also showed that the performance of the closed-loop case is higher than that of the open-loop case.

In the closed-loop case, circulating and oscillating regimes were observed. The difference of the performance between the two regimes is not large. The difference between two regimes could be explained by the motion behavior of fluid flow. And it could be simply described as: on the circulating flow, the fluid flow will travel in one direction; on the oscillating flow, the fluid flow will oscillate around a certain length.

Table 3. Summary of experimental results

| No | Date | Type | % | Hours | Q_cond (W) | Regime | Note |
|---|---|---|---|---|---|---|---|
| 10 | 2017-08-20 | Open-loop | 50 | 4 | NONE | Not working | Not working |
| 11 | 2017-08-22 | Open-loop | 50 | 4 | 176.487 | Oscillating flow | Stable |
| 12 | 2017-08-25 | Open-loop | 50 | 4 | 171.890 | Oscillating flow | Stable |
| 13 | 2017-08-27 | Open-loop | 50 | 4 | 175.227 | Oscillating flow | Stable |
| 14 | 2017-08-29 | Open-loop | 50 | 6 | NONE | Not working | Not working |
| 15 | 2017-08-31 | Open-loop | 50 | 4 | NONE | Not working | Not working |
| 16 | 2017-09-02 | Closed-loop | 60 | 3 | 180.659 | Oscillating flow | Stable |
| 17 | 2017-09-10 | Closed-loop | 60 | 4 | 189.582 | Circulating flow | Stable |
| 18 | 2017-09-17 | Closed-loop | 60 | 4 | 168.998 | Circulating flow | Reverse observe |
| 19 | 2017-10-22 | Closed-loop | 50 | 4 | 181.558 | Circulating flow | Stable |
| 20 | 2017-10-31 | Closed-loop | 50 | 4 | 186.073 | Circulating flow | Stable |
| 21 | 2017-11-07 | Closed-loop | 50 | 4 | 189.560 | Circulating flow | Stable |
| 22 | 2017-11-15 | Closed-loop | 60 | 4 | 173.289 | Oscillating flow | Stable |

### 3.3.3 Wall temperature and pulsating frequency

In the experiment, the values of wall temperature were used to evaluate the motion behavior of fluid flow at the time the fluid flow passed the measuring position. This data is normally affected by the liquid slug more than the vapor plug. Because the thermal conductivity of liquid is higher than vapor, the wall temperature changes obviously at the time the liquid slug passes the measuring position.

The temperature data was measured in two time: before-steady-state and steady-state. In the before-steady-state, data was recorded from the time we turned on the system until the time the system reached the state. In the steady-time, data was recorded for 1 hour from the time the system reached the steady.

Figure 7 shows the transition of temperature values respect to the time of the before-steady-state. It could be divided into 2 zones: not working and start-up zone. As we can see, on the not working zone, there is no motion until the time the heating water reached 67°C. By observing the other experiment data, the necessary temperature for the start-up of PHP is about 45°C for the distributed case (the liquid slug and vapor plug distribute scatter inside the tube) and 65°C for the separated case (the existence of the long liquid column and long vapor plug).

After the time the heating water reached 67°C, the value of wall temperature started to fluctuate and the difference of temperature between outlet and inlet water in cooling chamber gradually increase. Following time, with the increase of temperature of heating water, the flow regime changed from oscillating motion to circulating motion, as shown in Fig. 7. According to the results, this transition came from the change of motion behavior with the increase in temperature. The fluctuation of temperature around a certain temperature range represents for oscillating flow, and the fluctuation that wall temperatures were separated into two different range represents for the circulating flow. The difference between the two cases will be explained later.

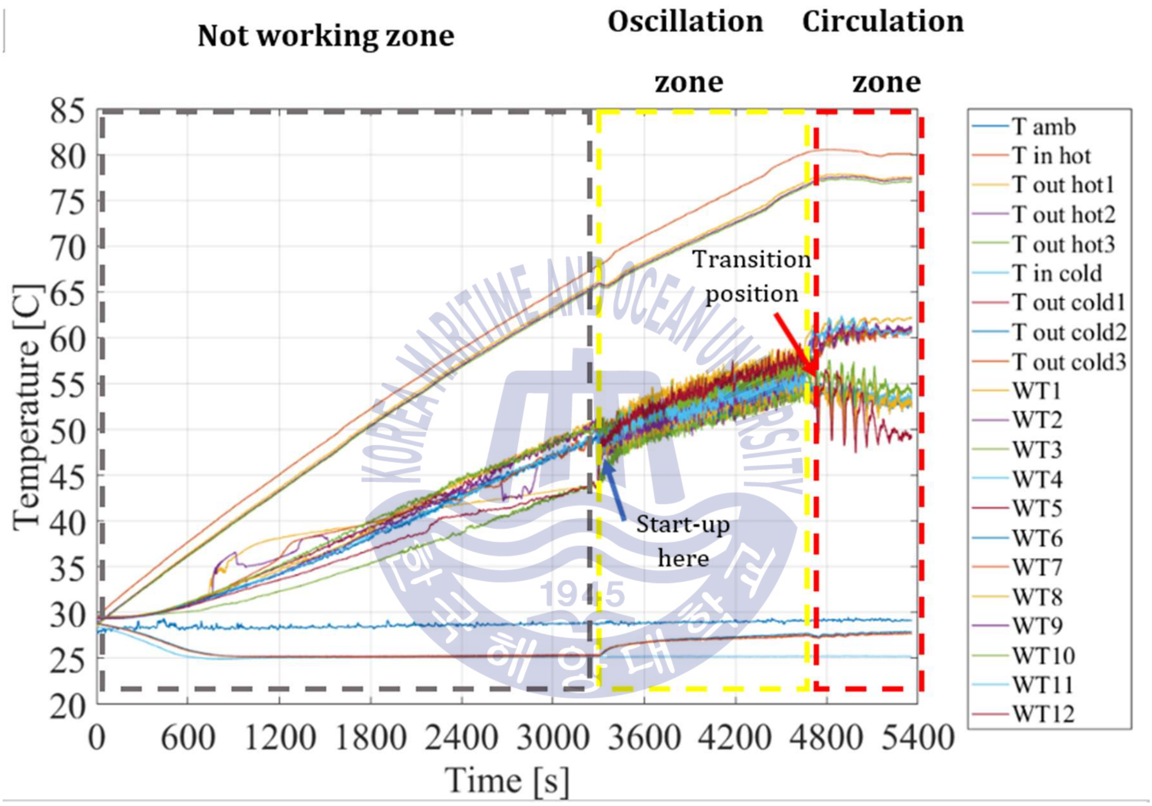


Figure 7. Wall temperature data of Test 19

Figure 8 illustrates the wall temperature at the steady state of the experiments (from 16 to 22). From the values of the odd and even tubes were displayed the red and blue lines to express the characteristic of motion. It could be mainly divided into two groups of regime: circulation (test 17, 18, 19, 20, 21) and oscillation (test 16 and 22). On the oscillating case, the wall temperature values fluctuated around the average temperature value of heating and cooling parts. However, on the circulating flow, the odd and even values fluctuated on two different ranges of temperature. The reason for the difference between two regimes is the motion behavior of fluid flow. On the circulating case, the fluid flows in one direction. Thus, the temperature of the points on the front of the heating section will high temperature and on the front of the cooling part will be low temperature. Otherwise, on the case of oscillating flow, the fluid flow oscillates around an uncertain length. Since that the values of temperature vary on an averaged range. It also indicated that the direction of motion could be determined by observing the difference of odd and even value, like the test 19, the even values higher than the odd values. It means that the direction of motion is anticlockwise.

Especially, the result also showed the reverse of the direction of fluid flow on test 18 and test 20. The reverse occurred many times in test 18 and it could be the reason for the reduction of the performance of PHP.

Overall, the motion of fluid flow in PHP is complicated and difficult to predict. The motion of PHP depends on the distribution of fluid flow inside the tube. The research found that by observing the wall temperature in the steady-state of the system, we can evaluate the operation and determine the regime of the system.

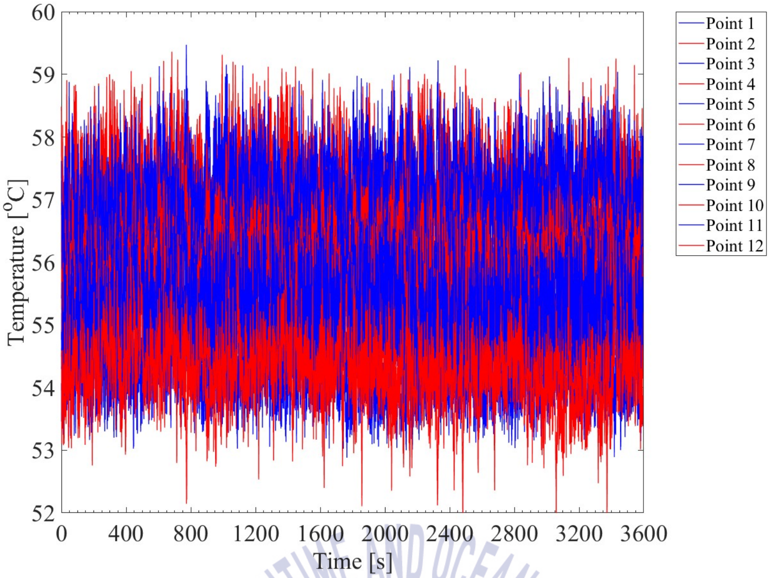


(a) Test 16

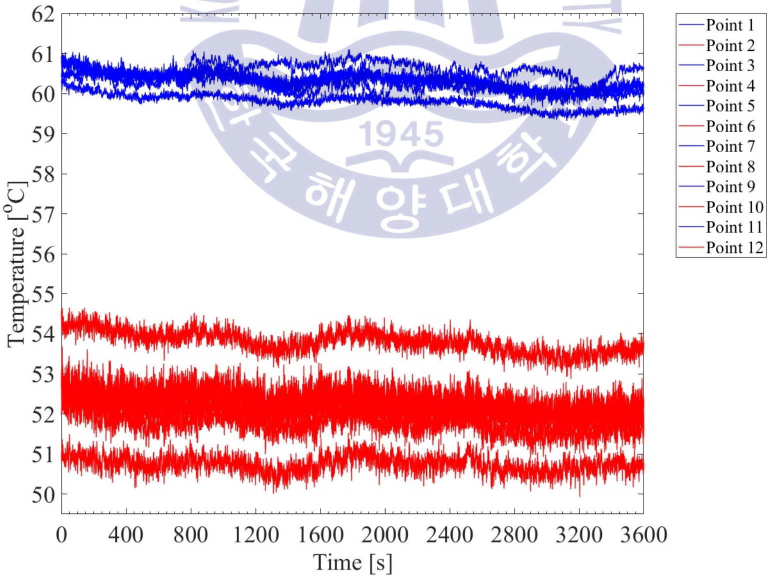


(b) Test 17

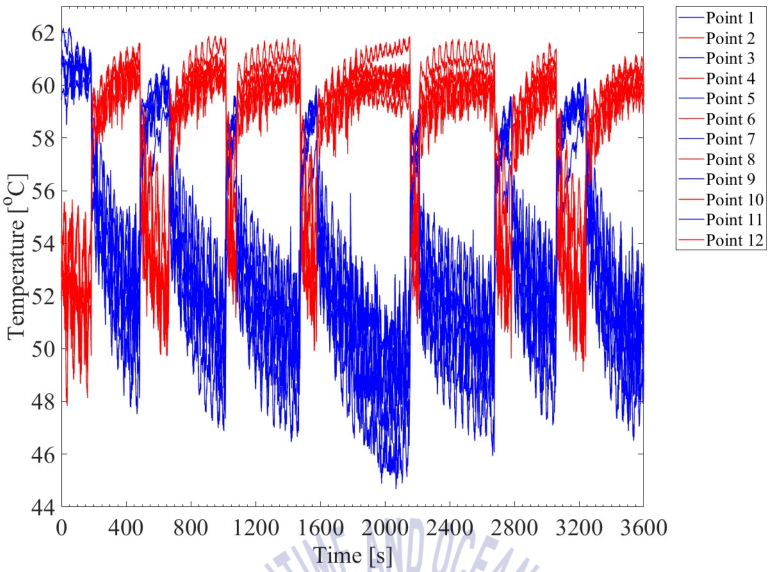


(c) Test 18

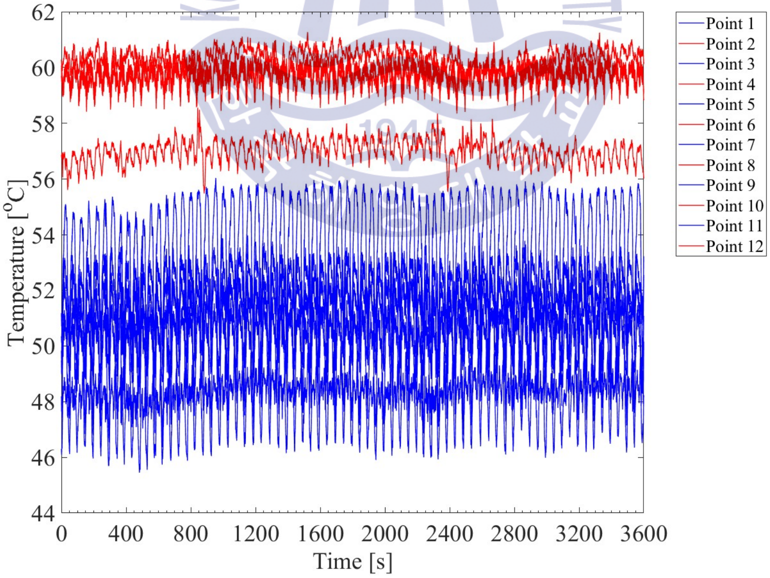


(d) Test 19

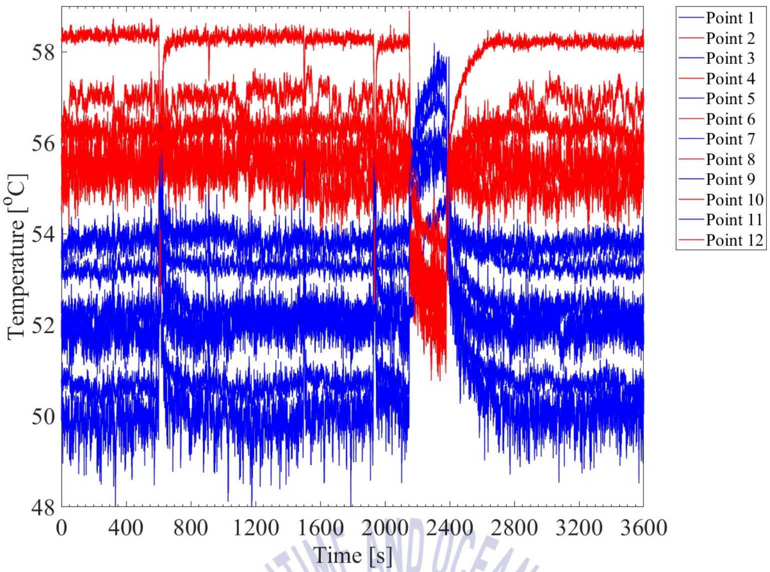


(e) Test 20

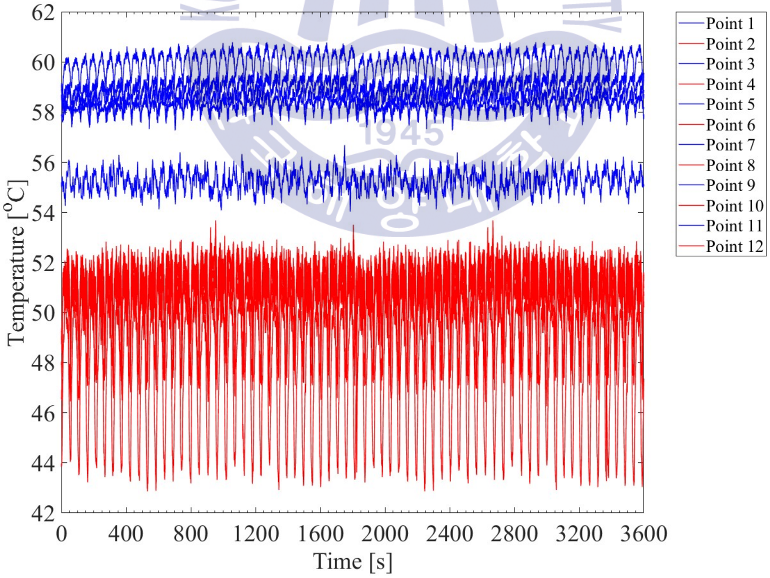


(f) Test 21

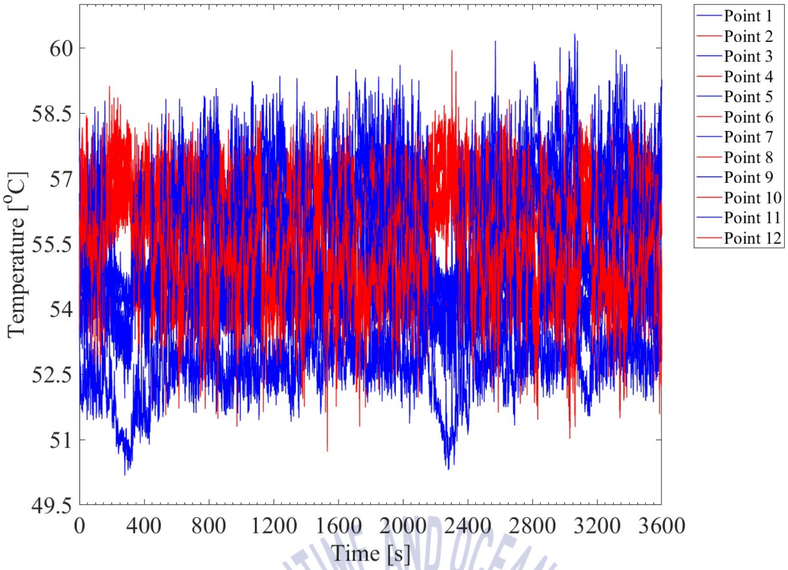


(g) Test 22

Figure 8. Wall temperature data (a) Test 16; (b) Test 17; (c) Test 18; (d) Test 19; (e) Test 20; (f) Test 21; (g) Test 22

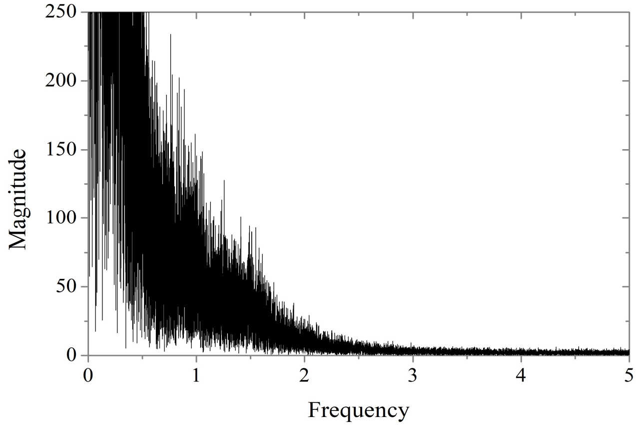


(a). Test 16

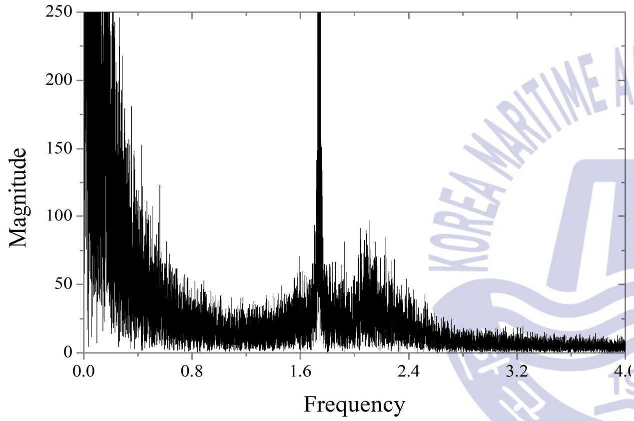


(b). Test 17

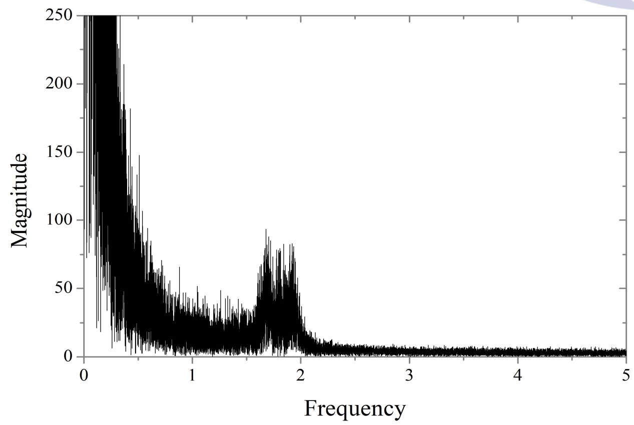


(c). Test 19

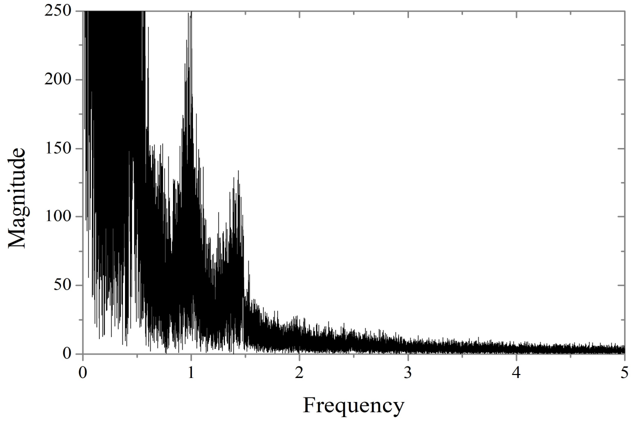


(d). Test 20

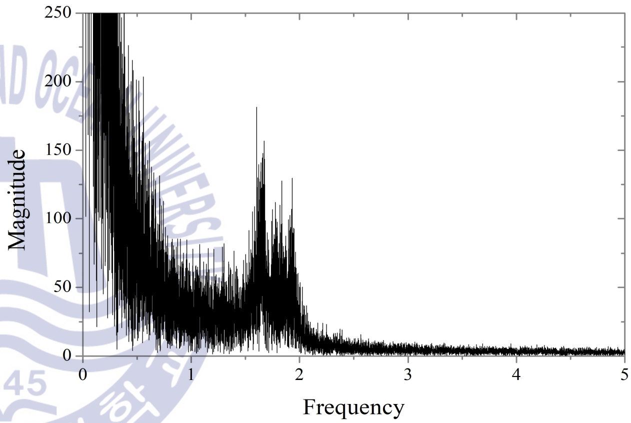


(e). Test 21

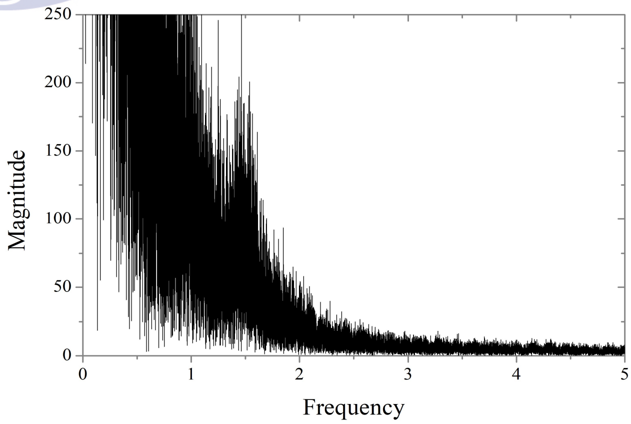


(f). Test 22

Figure 9. Fast Fourier Transform of temperature data

The FFT analysis was applied to investigate the frequency and amplitude of wall temperature of PHP. Figure 9 illustrates the frequency result of experiments. It is shown that only test 17 shown the existence of the period, and the value of test 17 is about 1.76 Hz. The other analysis results showed a wide range of frequency and the uncertain value. It indicated that the motion of fluid flow of PHP is complex and hard to predict.

### 3.3.4 Summary of experiment

The experiments investigating the operation of PHP using R123 as the working fluid was performed. It could be drawn as:

(1) The operation of the open-loop PHP is unstable and closed-loop PHP always is well-working. The performance of the closed-loop PHP is higher than the open-loop PHP. It is recommended that using the closed-loop structure for further study because of the stable operation and high performance.

(2) The wall temperature data showed the complication on the motion of fluid flow. The oscillating and circulating regimes were observed in this study. The wall temperature data indicated that with the increase of heat flux, the characteristic of motion will change from the oscillating to circulating flow. The difference of performance between the two regimes is not too much.

(3) The wall temperature also indicated that by observing this value, the regime of motion could be determined. The direction of motion of the circulating case also can be determined.

# Chapter 4 Numerical Analysis

## 4.1 Mathematical models

In this chapter, a numerical analysis for three-dimensional PHP as shown in Figure 10 is considered. According to the previous experimental studies [15, 35], the charging ratio in the range of 50-60% for R123 is suitable to achieve good thermal performance, which is highly attractive in real applications. The simulations were conducted for 2 cases: i) case 1: filling ratio (FR) = 50%, ii) case 2: FR = 60%. Table 1 showed the detailed configuration parameters of the investigated PHP. The present study uses Fluent v14.5 for investigation.

### 4.1.1 Governing equations

The previous study on visualization of PHP reveals that the flow pattern of fluid flow normally is related to the heat flux. When the heat flux is very low but enough to start PHP, the dominant flow pattern of the working fluid is the slug flow. Under this condition, the oscillation of the working fluid is quite random with very low velocity. As the heat flux becomes higher, the flow pattern will change to semi-annular flow and even the annular flow. Base on that, the Volume of fluid (VOF) is a compatible model to simulate PHP. The VOF model is a surface-tracking technique applied to a fixed Eulerian mesh. In the VOF method, the positions of vapor, liquid, and interface in the computational cells are represented by the volume fraction $\alpha_v$ and $\alpha_l$, where subscripts v and l represent vapor and liquid, respectively. The liquid phase exists in the cell where $\alpha_v = 0$

and the vapor phase occurs where $\alpha_l = 1$. Naturally, the vapor-liquid interface locates in the cell where $0 < \alpha_v < 1$. In each control volume, the volume fractions of all phases sum up to unity,

$$\alpha_v + \alpha_l = 1 \tag{4}$$

The tracking of the interface(s) between the phases is accomplished by the solution of a continuity equation for the volume fraction of one (or more) of the phases. For the phase, this equation has the following form

$$\frac{1}{\rho_q}\left[\frac{\partial}{\partial t}\left(\alpha_q\rho_q\right) + \nabla\left(\alpha_q\rho_q\vec{v}_q\right) = S_{\alpha_q} + \sum_{p=1}^{n}\left(\dot{m}_{pq} - \dot{m}_{qp}\right)\right] \tag{5}$$

where $\dot{m}_{qp}$ is the mass transfer from phase $q$ to phase $p$ and $\dot{m}_{qp}$ is the mass transfer from $p$ phase to phase q. By default, $S_{\alpha_q}$ is the source term on the right-hand side of equation (2) and equal zero.

*Momentum equations*

$$\frac{\partial}{\partial t}(\rho\vec{v}) + \nabla.(\rho\vec{v}\vec{v}) = -\nabla p + \nabla.[\mu(\nabla\vec{v} + \nabla\vec{v}^T)] + \rho\vec{g} + \vec{F} \tag{6}$$

The continuum surface force (CSF) model proposed by Brackbill et al. has been implemented such that the addition of surface tension to the VOF calculation results in a source term in the momentum equation. The general form of surface tension equation is the following:

$$F_{vol} = \sigma_{12}\frac{\rho k_1 \nabla\alpha_2}{\frac{1}{2}(\rho_1 + \rho_2)} \tag{7}$$

Where ρ is the volume-averaged density computed using Eq (10), Equation (11) show that the surface tension source term for a cell is proportional to the average density in the cell.

*Energy equations*

$$\frac{\partial}{\partial t}(\rho E) + \nabla.\left(\vec{v}(\rho E + p)\right) = \nabla.\left(k_{eff}\nabla T\right) + S_h \tag{8}$$

The VOF model treats energy, E, and temperature, T, as mass-averaged variables:

$$E = \frac{\sum_{q=1}^{n} \alpha_q \rho_q E_q}{\sum_{q=1}^{n} \alpha_q \rho_q} \tag{9}$$

where $E_q$ for each phase is based on the specific heat of that phase and the shared temperature.

The properties $\rho$ and $k_{eff}$ (effective thermal conductivity) are shared by the phases. The source term,$S_h$, contains contributions from radiation, as well as any other volumetric heat sources. The fluid properties in the above governing equations are determined by the presence of the component phases in each control volume,

$$\rho = \alpha_v \rho_v + (1 - \alpha_v)\rho_l \tag{10}$$

$$\mu = \alpha_v \mu_v + (1 - \alpha_v)\mu_l \tag{11}$$

### 4.1.2 Phase change model

The Ansys Fluent supports two models for simulating the interphase mass transfer through evaporation-condensation [16]. With the VOF formulations, only Lee model could be used. Lee developed a simplified saturation model for evaporation and condensation processes. The key premise of this model is that phase change is driven primarily by deviation of interfacial temperature from $T_{sat}$ and phase change rate is proportional to this deviation. Therefore, the phase change occurs while maintaining temperatures of the saturated phase and interface equal to $T_{sat}$.

The model assumes mass is transferred at constant pressure and quasi-thermo-equilibrium state according to the following relations:

If $T_l > T_{sat}$ (evaporation):

$$\dot{m}_{lv} = coeff * \alpha_l \rho_l \frac{(T_l - T_{sat})}{T_{sat}} \tag{12}$$

If $T_v < T_{sat}$ (condensation):

$$\dot{m}_{vl} = coeff * \alpha_v \rho_v \frac{(T_{sat} - T_v)}{T_{sat}} \tag{13}$$

### 4.1.3 Heat transfer model

When a fixed temperature condition is applied at the wall, the heat flux to the wall from a fluid cell is computed as

$$q = h_f(T_w - T_f) + q_{rad} \tag{14}$$

where

$h_f$ is the fluid-side local heat transfer coefficient.

In laminar flow, the fluid side heat transfer at walls is computed using Fourier's law applied at the walls. ANSYS Fluent uses its discrete form:

$$q = k_f \left(\frac{\partial T}{\partial n}\right)_{wall} \tag{15}$$

## 4.2 Geometry and mesh

### 4.2.1 Geometry model

The computational domain is modeled from the experimental test section. Figure 10 illustrates the configuration of the numerical model. To evaluate the operating of PHP, 12 points were chosen on the adiabatic region 1 for wall temperatures, and 47 points displayed by green color symbols were chosen along the length of the tube for pressure data.

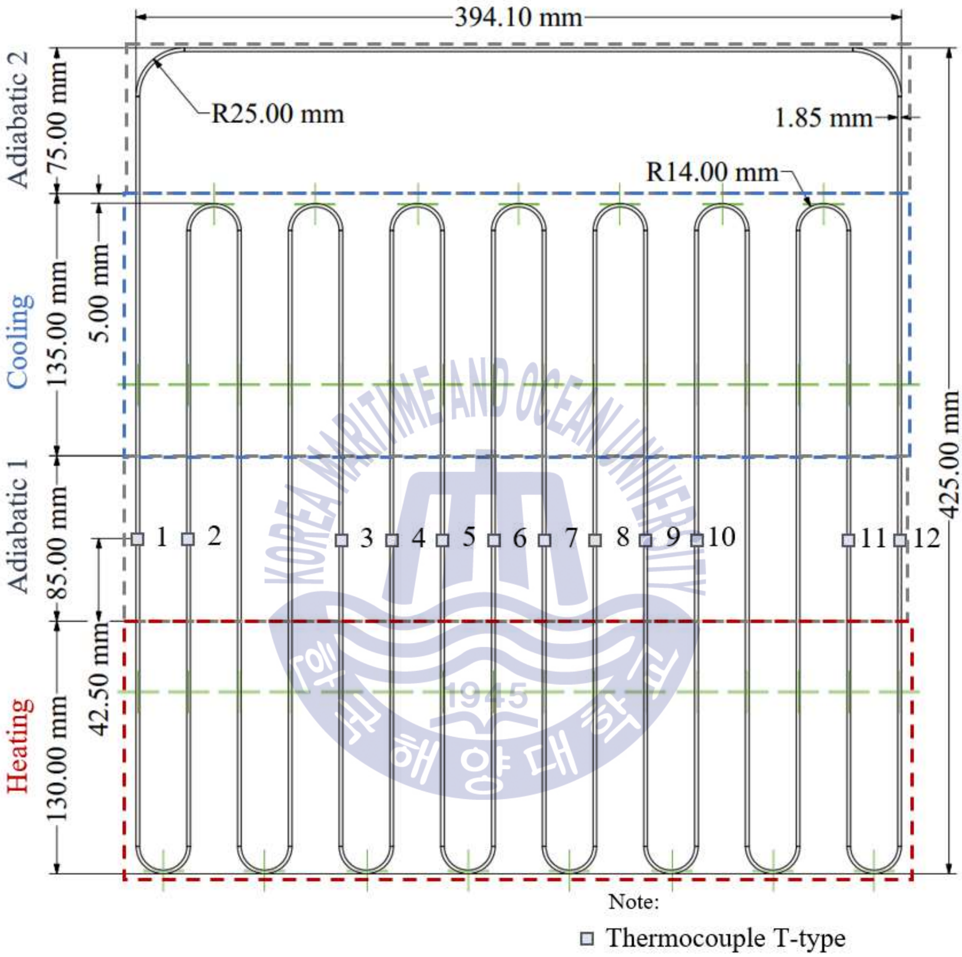


Figure 10. A model of PHP for numerical analysis

### 4.2.2 Meshing model

The configuration of the mesh could be examined in Figure 11. The quality of the mesh could be evaluated based on Skewness ratio. The details of meshing profile present on Table 4.

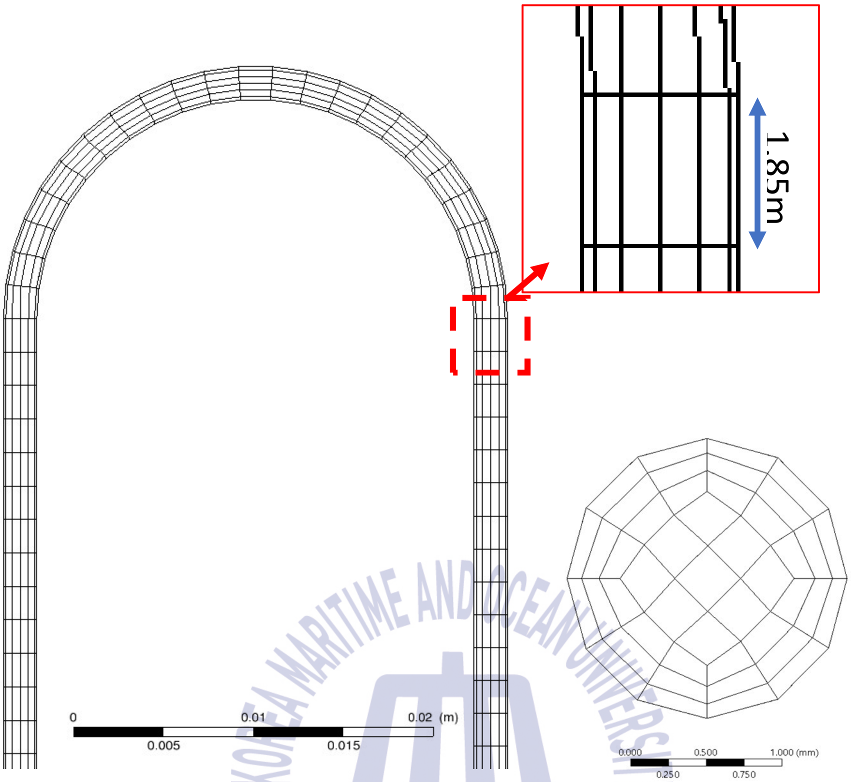


Figure 11. Meshing of bend

Table 4. Meshing profile

| Meshing profile | |
|---|---|
| Mesh type | Hexahedral |
| Number of nodes | 173992 |
| Number of elements | 150570 |
| Mesh quality –Mesh metric | Skewness |
| ▪ Min | 2.1e-6 |
| ▪ Max | 0.7212 |
| ▪ Average | 0.21886 |
| ▪ Standard Deviation | 0.10969 |

## 4.3 Initial and boundary conditions

The present simulation validated to accommodate with referenced experiment condition presented in this study. The constant temperatures were applied to the wall boundaries of condenser and evaporator. The values are 25ºC and 80ºC for cooling and heating parts, respectively.

The saturation temperature was provided as a function of pressure. The effects of the properties were also concerned. The ideal gas was applied to vapor density and the function of density respect to the variation of temperature was applied to the liquid density. The other properties have been set to equal with the properties of liquid and vapor at 50ºC. Table 5 presents the material properties of R123. The investigated setting above was employed on this study. Table 6 presents the summary of the setting condition.

The function of saturation temperature and liquid density:

$$T_{sat} = 263.9 + 4.6 \times 10^{-4}P - 1.2 \times 10^{-9}P^2 + 1.86 \times 10^{-15}P^3 - 1.2 \times 10^{-21}P^4 \quad (16)$$

$$\rho_L = 1867 + 2.4T - 0.0232T^2 + 5.47 \times 10^{-5}T^3 - 5.208 \times 10^{-8}T^4 \quad (17)$$

Table 5. Thermal-fluidic properties of R123 at 50°C

| Properties | Liquid | Vapor |
|---|---|---|
| Density ($kg/m^3$) | f(T) | Ideal gas |
| Special heat (J/kg-K) | 1051.9 | 744.83 |
| Thermal conductivity (W/m-K) | 0.069785 | 0.010698 |
| Viscosity (Pa-s) | 3.1588e-4 | 1.16e-5 |
| Surface tension (mN/m) | 12.281 | 12.281 |
| Enthalpy (J/kg) | 251060 | 411500 |

Table 6. Parameters for investigation

| Parameters | Value |
|---|---|
| Wall boundary temperature<br>▪ Heating<br>▪ Cooling | <br>80°C<br>25°C |
| Mass transfer<br>▪ Sat. temperature | <br>f(p) |
| Initial condition<br>Pressure<br>Temperature | <br>200000 Pa<br>321 K |

A random distribution of working fluid was initialized for both cases, as shown in Figure 12. The study showed that the start-up process of the random distribution occurred faster compared with the separated distribution (half of liquid and vapor locate at the bottom and top, respectively [33]). In this study, initial pressure and temperature values were set to equal with the values of R123 at 47°C.

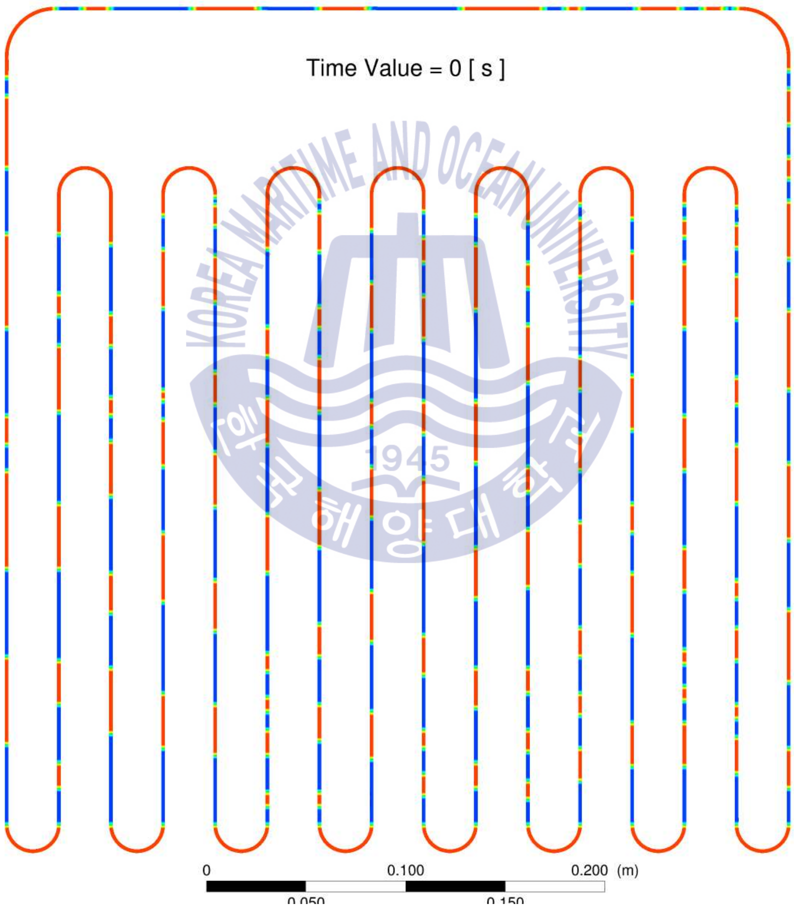


Figure 12. Initial distribution of fluid flow at t=0

## 4.4 Solution procedure

Furthermore, the pressure-velocity coupling is obtained by the semi-implicit method for pressure linked equations (SIMPLE) algorithm. The Body Force Weighted scheme is used for the pressure interpolation, and the first-order up-wind differencing scheme is adopted to discretize the momentum and energy equations. The second-order up-wind differencing scheme is adopted to discretize the density equation. The Compressive interface reconstruction technique is used to track the geometry of the interface.

The resulting system of algebraic equations is solved using the Gauss–Seidal iterative technique in conjunction with an algebraic multigrid (AMG) method, with successive under-relaxation to improve the convergence properties. The simulation test indicated that a good convergence is performed if the under-relaxation factors are used with the values: 0.3 (pressure), 1 (density), 1 (body force), 0.7 (momentum), and 1 (energy).

Moreover, the residual criterion is also concerned in the convergence study. The solution of every calculated item (i.e. continuity, velocities, and energy) is assumed to converge when residual of each item is less than the corresponding residual criterion. The global Courant Number (a dimensionless number that compares the time step to the characteristic time of transit of a fluid element across a control volume) is less than 0.3 in every time step, which can guarantee the good convergence and solution precisions.

Considering the computing cost and accuracy of numerical results as mentioned above, our computational results are presented in case of cell number 150570, computational time step $1 \times 10^{-4}$ s, and residual criteria:

$1 \times 10^{-3}$ for continuity, $1 \times 10^{-3}$ for velocities, and $1 \times 10^{-6}$ for energy. In addition, the relevant integrated quantities and heat and mass balances are also checked at each time step to ensure the convergence of numerical results. The summary of the setting shown in table 7.

Table 7. Summary of model setting

| **Parameter/ Models** | **Settings** |
|---|---|
| Spatial and time settings | Gravity activated |
| Solver | Pressure based solver<br>Absolute velocity formation<br>Unsteady state analysis |
| Multiphase model<br>▪ Volume of fluid | Active with two phases:<br>▪ Phase liquid and vapor<br>Volume fraction<br>▪ Explicit scheme<br>▪ Zonal Discretization activated<br>Implicit Body forces activated |
| Energy equation | Activated |
| Viscous model -Laminar | ▪ Viscous heating activated |
| Solution setting<br>▪ Time step size<br>▪ Number of time step<br>▪ Max Iteration | <br>0.0001<br>200000<br>200 |
| Solution Controls –URF<br>▪ Pressure<br>▪ Density<br>▪ Body Forces<br>▪ Momentum<br>▪ Vaporization Mass<br>▪ Energy | <br>0.3<br>1<br>1<br>0.7<br>1<br>1 |

## 4.5 Results and discussions

The numerical simulation and experiment were conducted on two-case with variable charging ratio: 50 and 60%. The case FR = 50% and FR = 60% will be named case 1 and case 2, respectively. The research showed that the circulating flow regime with periodicity feature was also observed in both experiment and simulation. The results about flow pattern, wall temperature, and heat transfer rate were analyzed and compared with experimental data to understand the mechanism of PHP. Additionally, the pressure values along the length of the tube were processed to obtain surface graphs.

### 4.5.1 Circulating flow in PHP

In the present study, the circulating motion behavior of PHP will analyze on one period of motion of numerical result to understand better about characteristic of motion. The researcher was choice five flow pattern contours in 5 special times of a period of motion with FR = 50% to analyze and compare with experiment visualization of test 19. The compared picture is using the visualization of 2 turns on the final right-side, as shown in Figure 13. Additionally, the pressure data along the length of the tube at the times above were also processed to parallel analyze with flow pattern contours to explain the mechanism of this regime.

Figure 13 illustrates the volume fraction of liquid and vapor at the different time in a period of motion and Figure 14 depicts the pressure data at the different time of the selected period. The period was chosen in a range from t = 10.54 s to t = 12.58 s. This period was chosen in the time the motion reached the steady state, as shown on the Figure 17 (a). The initial time of the period was analyzed at the time of the liquid column locating on the tube 17th start moving downward, and the ending time was chosen at the time the regeneration time of liquid column to complete a cycle. Before present about the motion of fluid flow, it should be noted that the main characteristic of motion is the travel, regeneration, and separation of the long liquid columns inside the tube. These long liquid columns with the short vapor plugs located inside could be examined in Figure 13 (a).

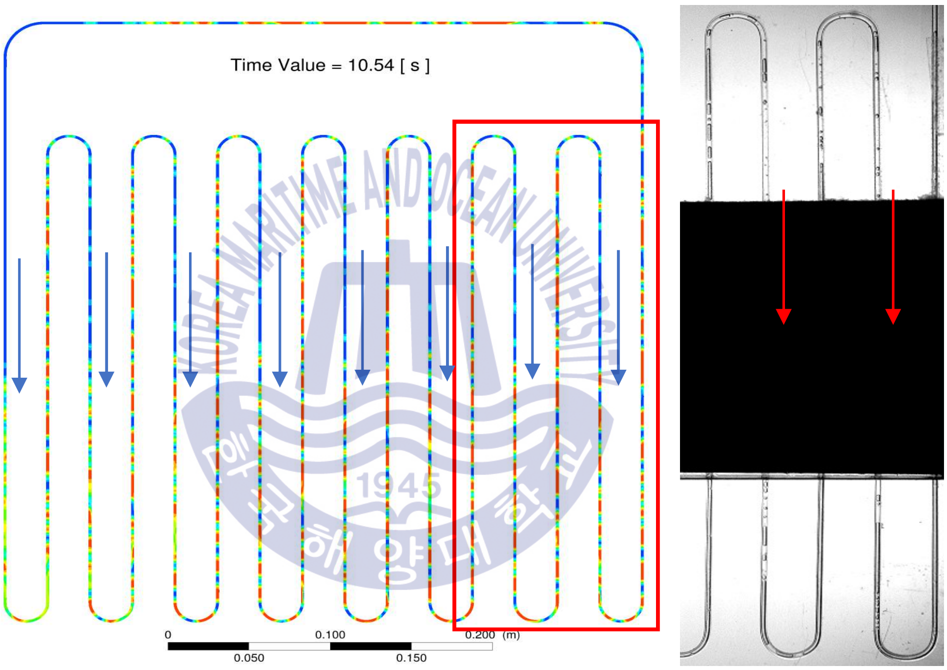


(a) Liquid-vapor distribution at t_sim = 10.54 s

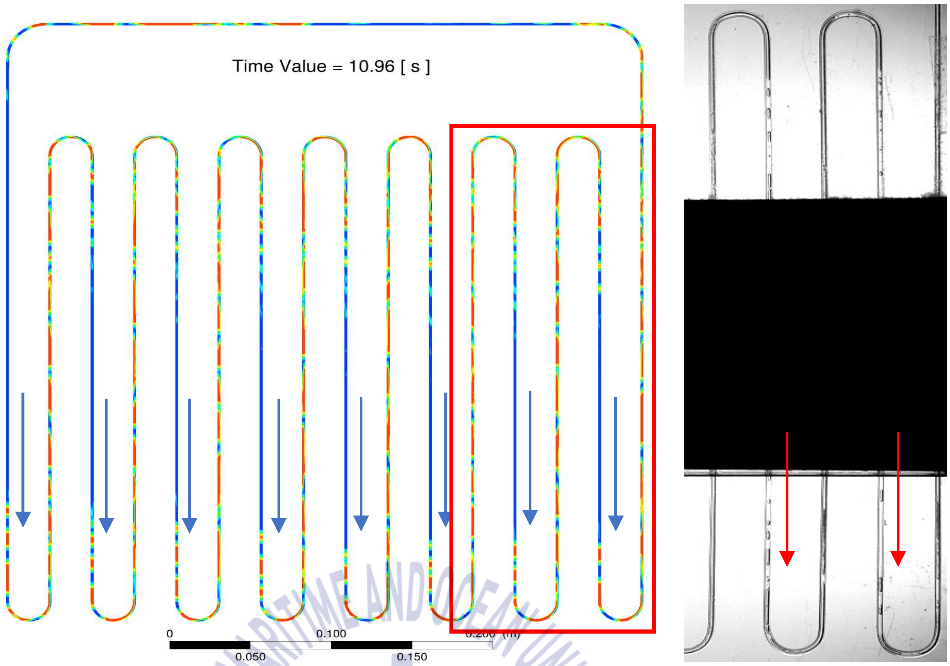


(b) Liquid-vapor distribution at t_sim = 10.94 s

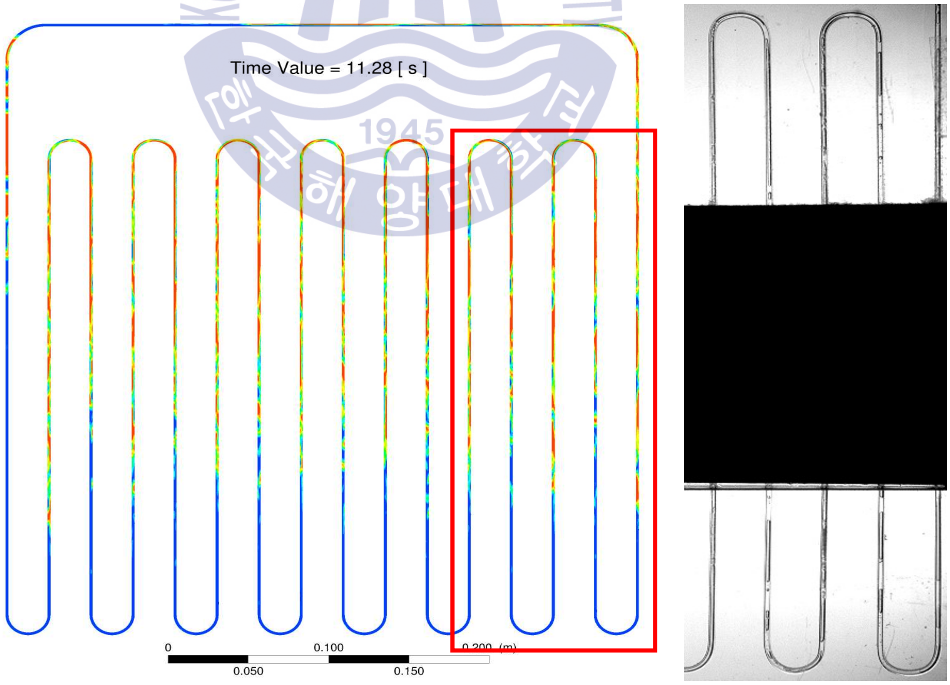


(c) Liquid-vapor distribution at t_sim = 11.28 s

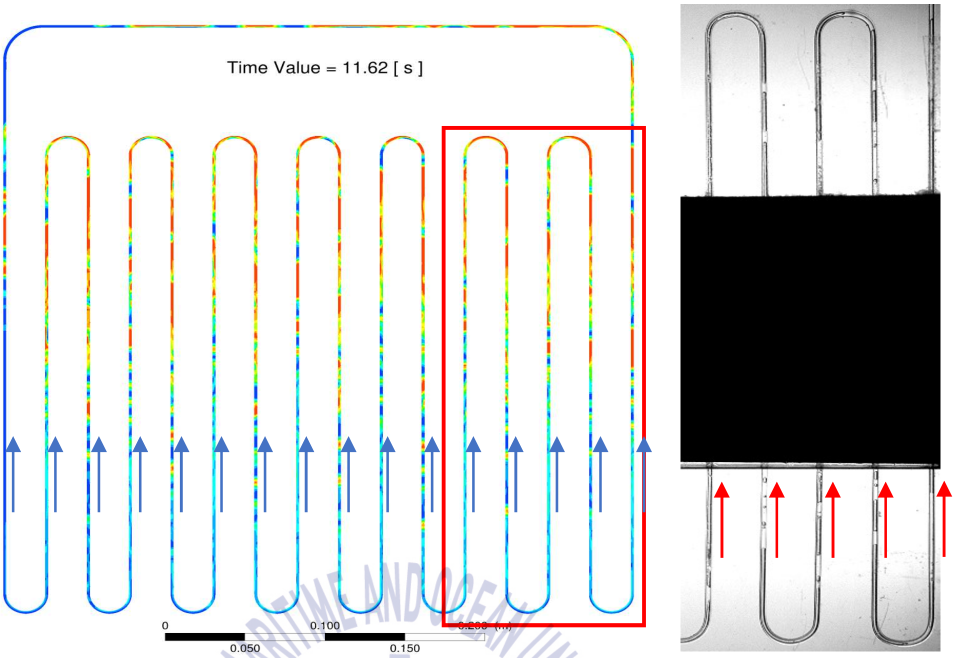


(d) Liquid-vapor distribution at t_sim = 11.62 s

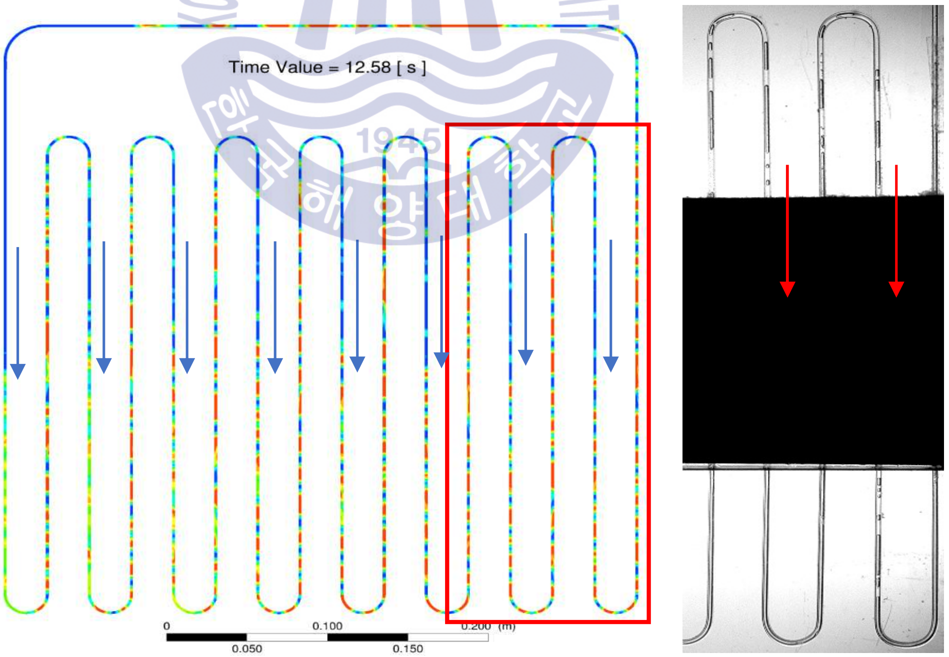


(e) Liquid-vapor distribution at t_sim = 12.58 s

Figure 13. Motion on one period of case FR =50% compared with Test 19

As shown in Figure 13 (a), at t = 10.54 s, the location of long liquid columns on the top U-bend could be examined in both visual experiment and simulation. At this time, these liquid columns have a trend to go downward. The reason comes from the slight difference of the pressure between the left-side and right-side tubes and the effect of gravitation. As shown in Figure 14, the pressure value of the left-side tube is higher than the right-side tube. Hence, the liquid columns had a trend to travel on anti-clockwise direction. It also should be known that, before this time, the entire pressure still increases and will reaches the peak at the next time (t = 10.94 s), as shown in Figure 14.

At t = 10.94 s, the liquid columns are on the way to move downward and push the vapor plugs to go upward, as shown in Figure 13 (b). There vapor plugs contact with the cooling section and the condensation process occur. Because of this process, the entire pressure of PHP system will reduce, as shown in Figure 14. The similar motion behavior also observed in the experiment.

At t = 11.28 s, all liquid columns have totally moved downward and located at the bottom U-bend. Vapor plugs had been pushed to go upward. In this time the pressure along the length reduce and vary in the range from 262.5 kPa to 266 kPa, could be examined in Figure 14. The slightly difference between the left and right side could be observed.

At t = 11.62 s, the boiling process occurs at the bottom. The liquid columns have been separated into two liquid columns with the dispersed bubbles at the separated location. Because of the boiling, the pressure at the bottom U-bend increase and push the separated liquid column go upward on two directions, as shown in Figure 14.

At t = 12.58 s, the recombination of the liquid column happens. The liquid column which was separated and go upward on the anti-clockwise direction will combine with the separated liquid column of the right adjacent tube. The long liquid columns regenerate on the top U-bend as shown in Figure 13 (e). The period of a cycle complete. The periodic motion occurs during the 20s and clearly expressed in the wall temperature and heat transfer rate results.

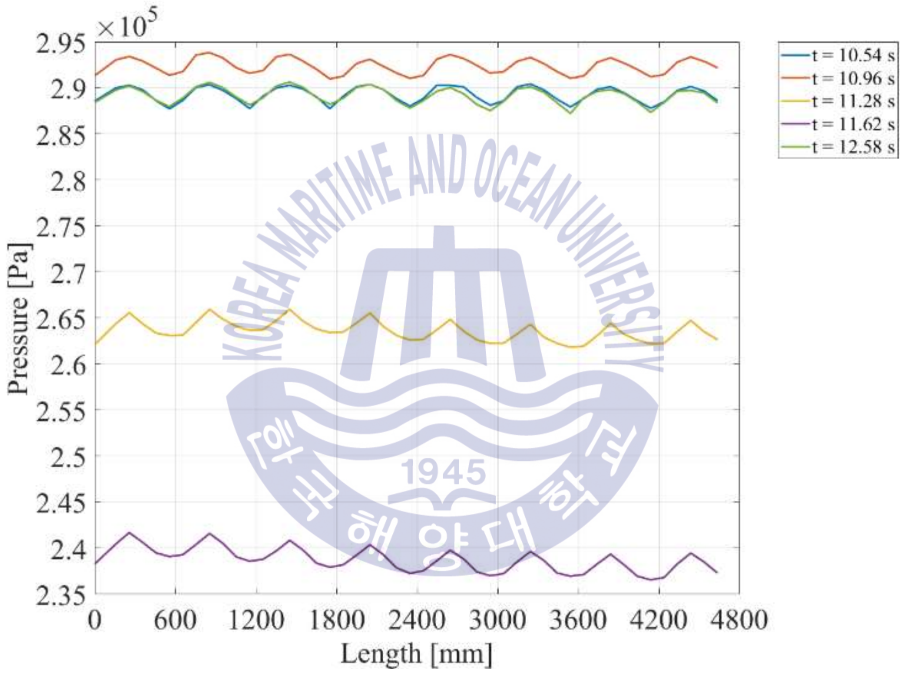


Figure 14. Pressure distribution along tube length at selected time

### 4.5.2 Wall temperature

In the experiment, the wall temperature normally is used to evaluate the motion behavior of fluid flow. It presents for the temperature value of fluid flow at the time the fluid flow across the measured position. And this value could be strongly affected by the liquid, because of the thermal conductivity of liquid higher than vapor.

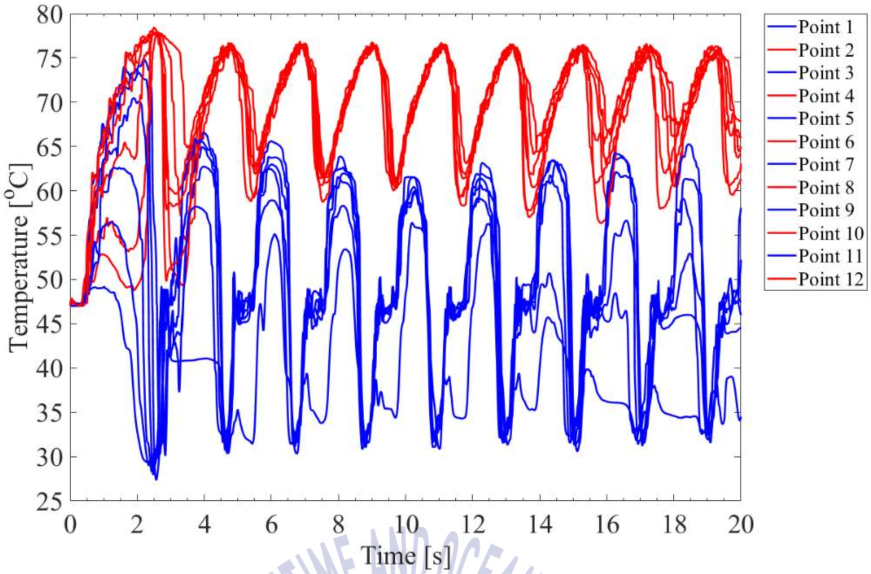


(a) Wall temperature of simulation of case 1

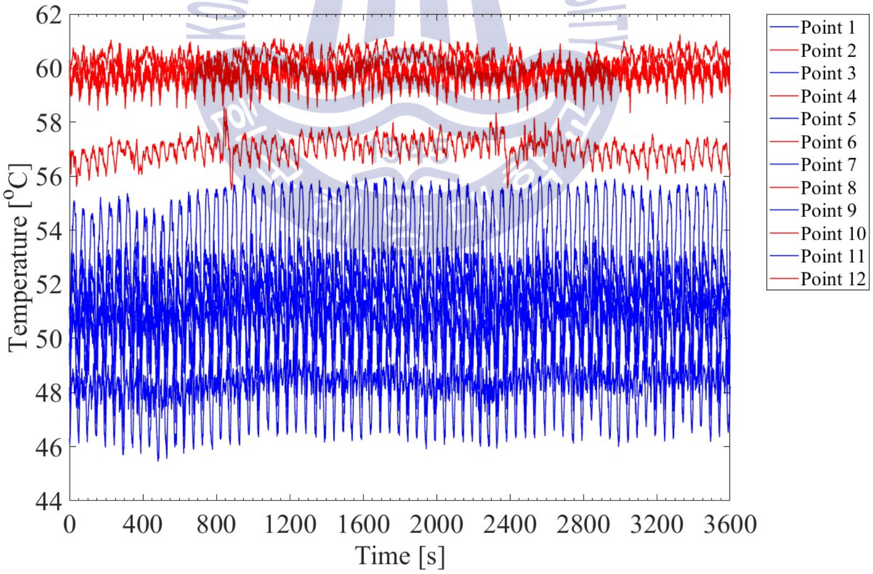


(b) Wall temperature of test 19

Figure 15. Comparison of wall temperature between (a) simulation and (b) experiment for charge ratio of 50%.

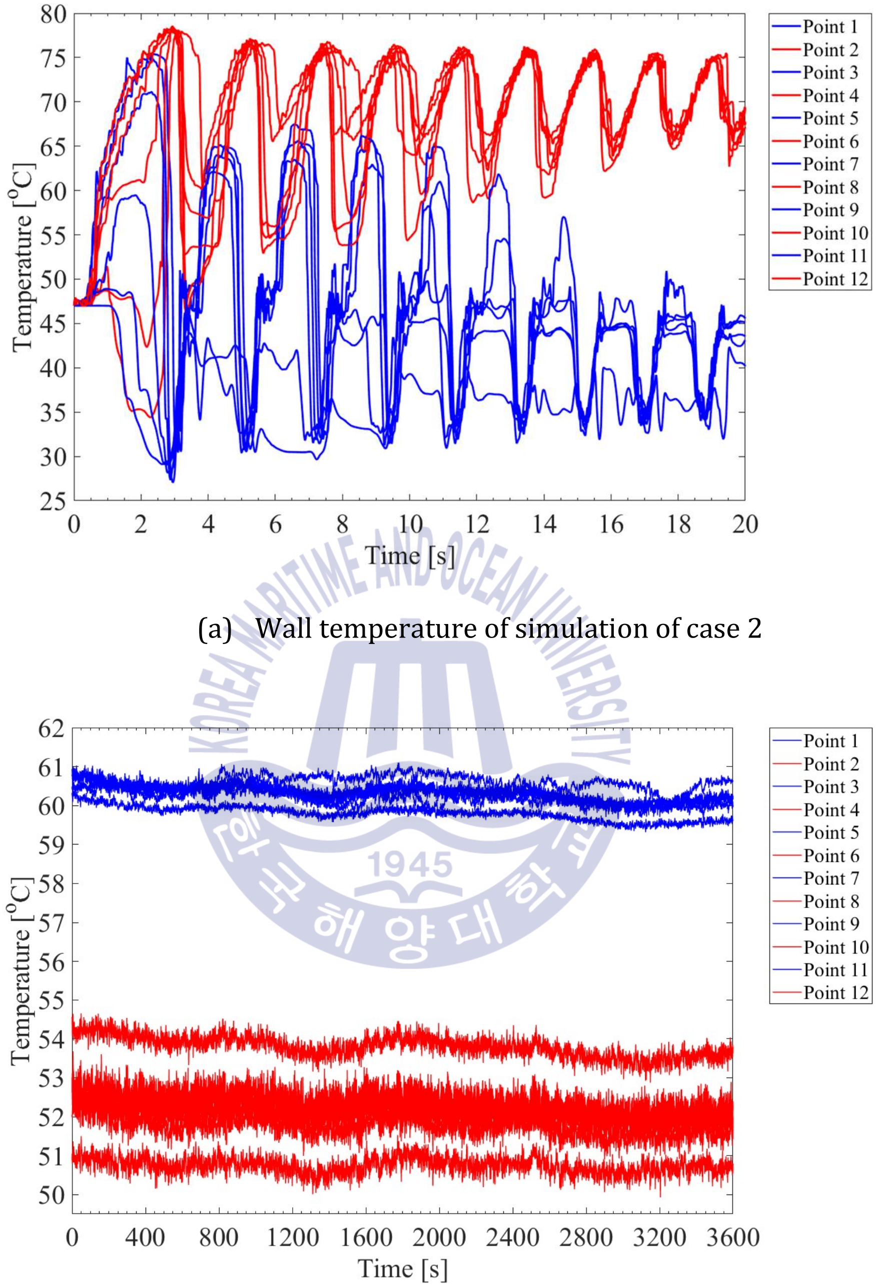


(a) Wall temperature of simulation of case 2

(b) Wall temperature of test 17

Figure 16. Comparison of wall temperature value between (a) simulation and (b) experiment for charge ratio of 60%

Figure 15 and 16 show the comparison of wall temperature between the experiment and simulation with the varied charging ratio. The temperature data of the experiment was recorded in 1 hour in the time the system operates stability, as shown in Figure 15 (b) and Figure 16 (b). There were compared with the data of simulation of Figure 15 (a) and Figure 16 (b).

The results showed the agreement about the fluctuated feature of wall temperature. The lines representing for the odd and even point was displayed by blue and red color to point out the feature of fluctuation. Specifically, the even and odd value fluctuate around two different range of temperature. As shown in Figure 15 and 16, the series of odd value fluctuate in the range which is lower than the range of even value in both of experiment and simulation.

The difference in the range of temperature could be explained by the characteristic of circulating motion. It could figure out that the temperature value of fluid flow after it across the heating section will higher than the temperature value of fluid flow across the cooling section. It also had been seen that the fluid flow travels on the anti-clockwise in both experiment and simulation. Thus, the even values always fluctuate on the high range of temperature than the odd values. This feature indicates that by observing the wall temperature value at the adiabatic section, we can find out the regime of motion or the direction of motion. It could be seen that the results of figure 15 (a), (b) and figure 16 (a) move counterclockwise and figure 16 (b) move clockwise. The data also showed the difference about the amplitude between odd and even values. The difference of fluctuating amplitude also observed in the experiment results. The cause comes from the complication of motion.

### 4.5.3 Heat transfer rate

Figure 17 illustrates the cooling and heating heat transfer rates of two cases with different charging ratio. The results above obtain by integrating the heat flux through the evaporating and condensing surface. Generally, the heat transfer rate of the heating and cooling fluctuate with the amplitude is obvious and steady. Especially, an exciting feature of the variation of the heat transfer rate was observed in this study. As we can see that, the fluctuating amplitude of the heating is largely higher than the cooling. It could be explained by analyzing the motion of fluid flow at a special point like the trough and peak of a steady period. Figure 13 (a-d) will reuse to explain for the feature above of fluctuating amplitude of the heating and cooling.

Figure 13 (c) depicts the void fraction at the time the heating heat transfer rate reach the peak, t =11.28 s. It could be seen that at this time almost liquid columns totally locate at the bottom. Before this time, these liquid columns locate on the top section and tend to travel downward the bot section. Thus, in the time these liquid columns travel to the bot section, the heat transfer rate will increase and reach the peak at the time all the columns locate at the bot section. Because the thermal conductivity of the liquid is higher than vapor and the high difference between the wall and liquid temperature since the heat transfer at this time will be highest.

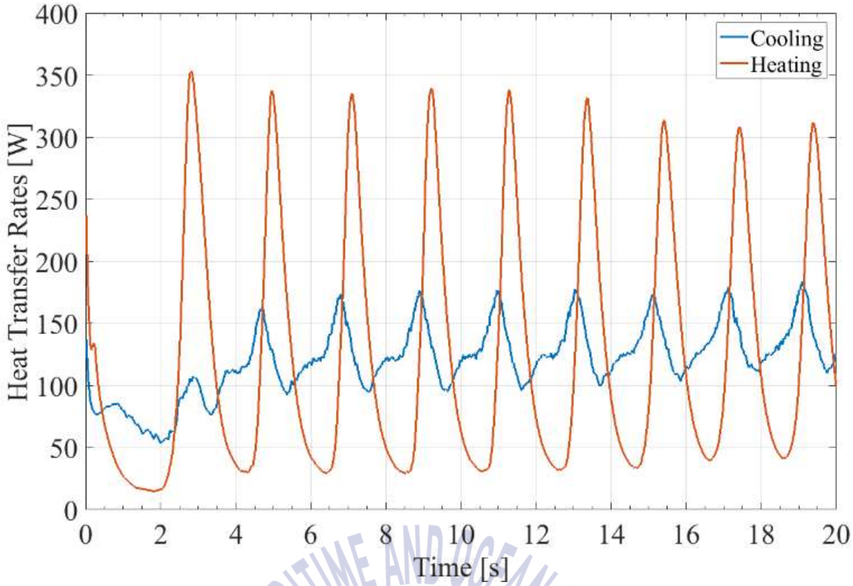


(a)

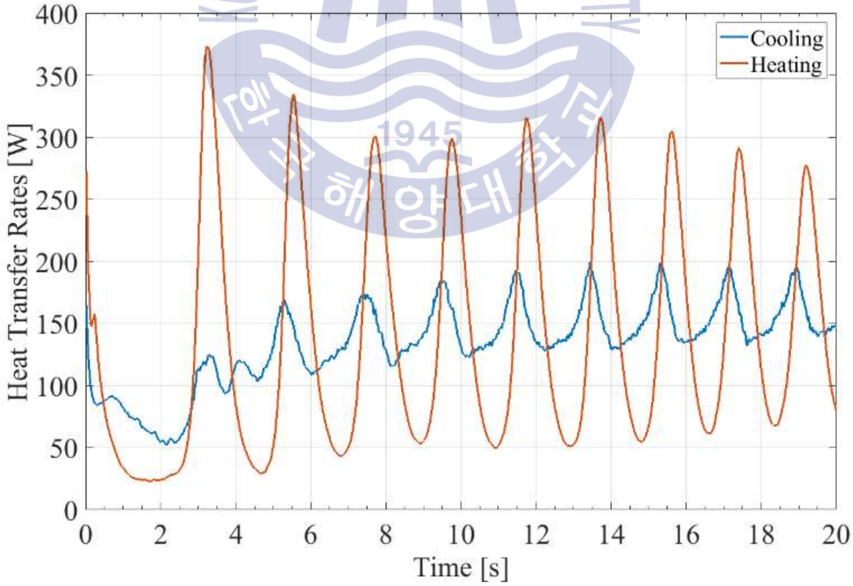


(b)

Figure 17. Heat transfer rates in cooling and heating parts of (a) FR = 50% and (b) 60%

On the other way, the heat transfer rate of the heating reduces to the trough in the time the liquid columns were pushed upward to the top section and only the vapor plugs located at the bottom section, as shown in Figure 13 (a). At this moment, the heat transfer rate of the heating will be the lowest because of the small difference between the wall and inside fluid temperature and also because of the low thermal conductivity of vapor.

On the case of cooling, the heat transfer rate increases in the time the vapor columns travel upward and reach the peak at the time almost the vapor columns locate at the top section, as shown in Figure 13 (b). It could be figured out that the peak of the cooling is lower than the heating because the thermal conductivity of vapor is lower than liquid even the difference of temperature between the vapor and wall is high. Figure 13 (d) shows the distribution of fluid flow at the time the heat transfer rate of the cooling decrease to the trough. Different from the cases above, the changing of motion behavior is more complex. It could be described like on a short time after the value reaches the peak, then the heat transfer rate reduces sharply caused by the condenser process. On the next time, the liquid column which separated from the long liquid column by the boiling process will move upward and the heat transfer rate will increase directly. The slope of the data on the right of the peak is sharper than the left. Consequently, the heat transfer occurs continuously by the moving of the separated liquid column and the rising of vapor plus at the high temperature.

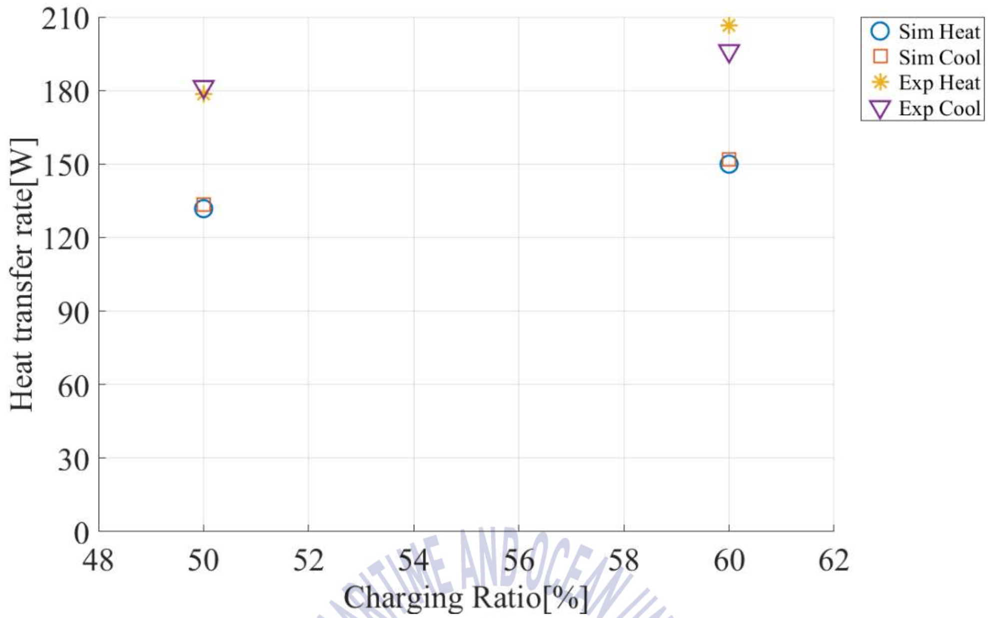


Figure 18. Comparison of heat transfer rate between simulation and experiment for two cases of FR = 50% and 60%

Moreover, there is a small difference in the fluctuation amplitude between the two cases. It could be seen that the peak of the periods of the case 1 is higher than case 2. However, the trough of the case 1 is lower than case 2. The heat transfer rate of heating and cooling were calculated by integrating the 5 periods of motion in the steady-state and compared with the heat transfer rate calculated from the experiment. Figure 18 shows the comparison of the heat transfer rate between simulation and experiment, respectively.

The results show that with the increase of the charging ratio, the heat transfer rate also increases in both experiment and simulation. The heat transfer rate for the case FR = 60% is higher the case FR = 50%. However, there still have a big difference between numerical predict experimental results.

### 4.5.4 Pressure data

Pressure values at 47 points which distribute along length of tube were chosen to create a surface graph. Figure 19 illustrates the transient of pressure value along the length of tube respect to the time. It was found that the pressure values along length will simultaneously change correspond with the moving of the fluid flow and this change has a periodicity feature. The results indicated that there is a relationship between the motion of fluid flow and pressure. The consequence of motion above obtained by employing the ideal gas for vapor and a function for liquid density. And using the function respect to the pressure for saturated temperature.

Specifically, the pressure value will reduce in the time the liquid columns travel to the bottom U-bend. Because in this time, the liquid columns will push the vapor columns to upward. At the time the vapor contact with cooling surface, the condensation process occurs on the top section, as shown in Figure 13(b). Hence, the pressure along the length will decline immediately. Contrastingly, these series values of pressure will increase rapidly when the liquid column located at the U-bend start to vaporize. Since this is a closed system, the entire pressure inside the tube will rise until the time the liquid columns regenerate and travel downward.

The difference of the amplitude respect to the time of the pressure between two cases can easily recognize. In case 1, the value of pressure along the length varies on the stability range. On the other hand, the value of case 2 varies with the amplitude gradually become steady follow time. The range of fluctuation is about from 243kPa to 296 kPa.

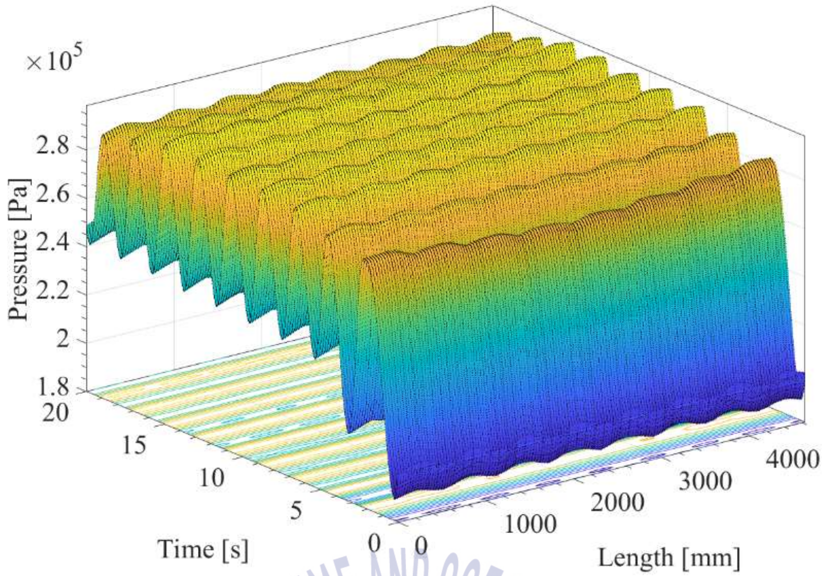


(a) FR =50%

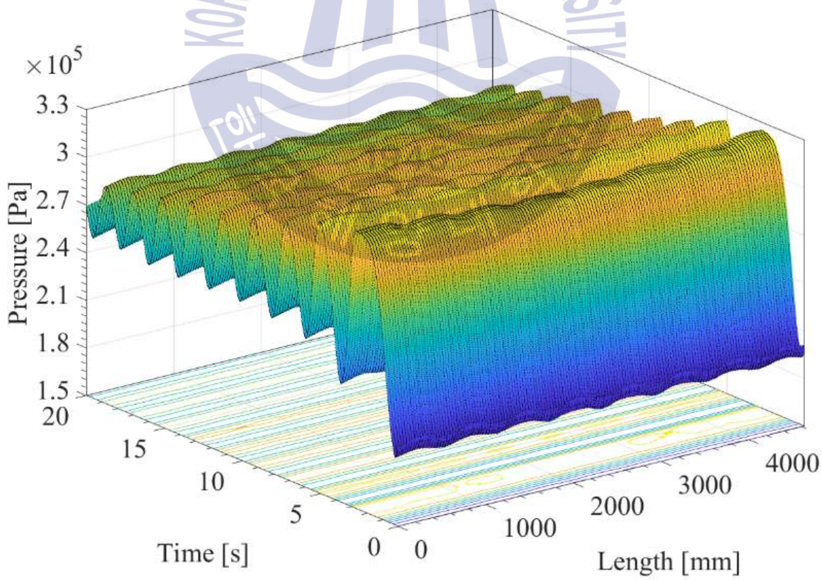


(b) FR = 60%

Figure 19. Transient behavior of pressure along length of tube in (a) FR = 50 % and (b) FR = 60 %

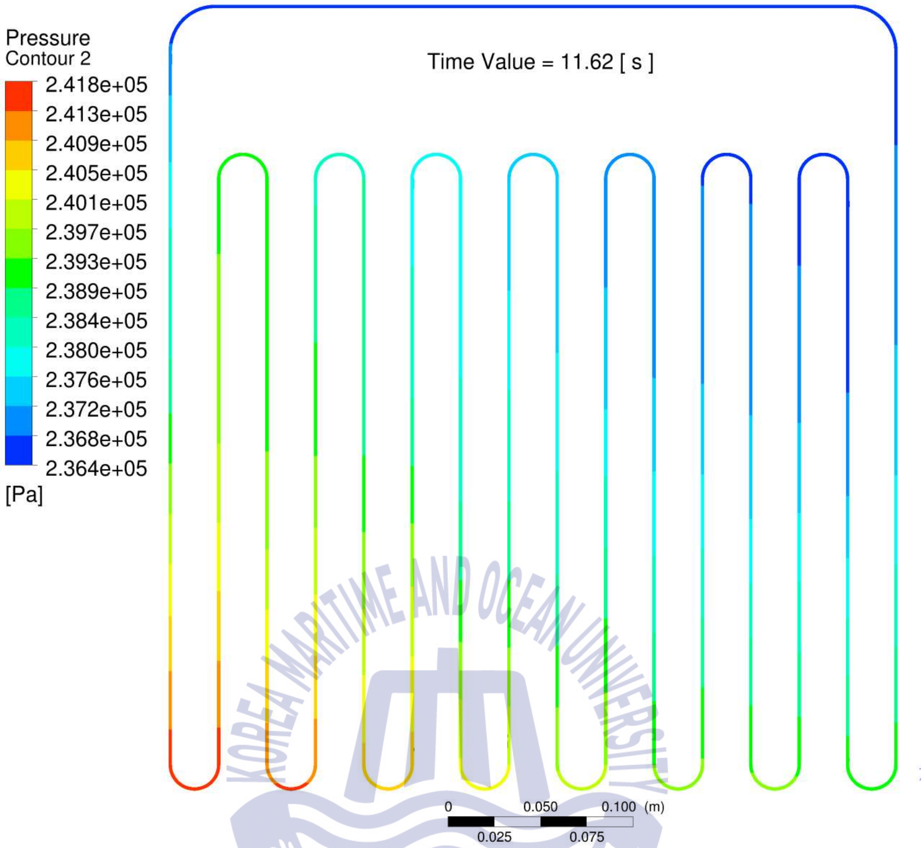


Figure 20. Pressure contour at t = 11.62 s

Furthermore, the current study also reveals that the travel in one direction of motion comes from the difference of pressure between the left and right side. Figure 20 displays the pressure contour at the time t = 11.62 s. It could be seen that the pressure of the left-side tubes is higher than the right-side tubes. It leads to the motion direction to the anti-clockwise on this simulation.

# Chapter 5 Conclusion

In the present study, the experiment and simulation of pulsating heat pipe were performed to investigate the motion behavior of the fluid flow with a varied charging ratio of 50% and 60% with the working fluid is R123. The constant temperature boundary conditions were applied to evaporator and condenser, respectively. The circulation motion was observed in both simulation and experiment. The results of the wall temperature, heat transfer rate and flow pattern of simulation were analyzed and evaluated to understand better about the mechanism of PHP. The study could be drawn as:

(1) The regime of fluid flow could be determined based on the wall temperature of two adjacent tubes at the adiabatic region. Especially, on the circulation regime case, the temperature value of even and odd tube fluctuates on difference range.

(2) The operation of open-loop PHP is unstable. It is recommended to use closed-loop PHP for further study.

(3) The characteristic of R123 is suitable to apply for the micro-PHP.

(4) The properties of density and saturated temperature applied to the Lee model should be supplied as a variation value.

(5) The values of pressure along the length of the tube change with the motion of fluid flow. And the direction of motion caused by the difference of pressure between the left-side and right-side tubes.

(6) The numerical results lead out the heat transfer rate of the heating section normally fluctuates with high amplitude compared with heat transfer rate of the cooling section.

# References


[1] H. Akachi, F Polasek, P Stulc, Pulsating heat pipes, International Heat Pipe Symposium, pp. 208-217,1996.

[2] P. Charoensawan, S Khandekar, M Groll, P Terdtoon, Closed loop pulsating heat pipe Part A: parametric experimental investigations, Applied Thermal Engineering, 23, 2009-2020, 2003.

[3] S. Khandekar, N. Dollinger, M. Groll, Understanding operational regimes of closed loop pulsating heat pipes: an experimental study, Applied Thermal Engineering, 23, 707-719, 2003.

[4] H. Yang, S. Khandekar, M. Groll, Operational limit of closed loop pulsating heat pipes, Applied Thermal Engineering 28, 49-59, 2008.

[5] Y Zhang, A Faghri, Advances and unsolved issues in pulsating heat pipes, Heat Transfer Eng, 29, 20-44, 2008.

[6] X. Han, X. Wang, H. Zheng, X. Xu, G. Chen, Review of the development of pulsating heat pipe for heat dissipation, Renewable and Sustainable Energy Reviews, 59, 692-709, 2016

[7] J. Qu, H. Wu, P. Cheng, Start-up heat transfer and flow characteristics of silicon-based micro pulsating heat pipes, Int J Heat Mass Transf, 55:6109–6120, 2012.

[8] H. Yang, S. Khandekar, M. Groll, Performance characteristics of pulsating heat pipes as integral thermal spreaders, Int J Therm Sci, 48,815–824, 2009.

[9] P. Charoensawan, P. Terdtoon, Thermal performance of horizontal closed-loop oscillating heat pipes, Appl Therm Eng,28,460–466, 2008.

[10] S. Rittidech, P. Terdtoon, M. Murakami, P. Kamonpet, W. Jompakdee, Correlation to predict heat transfer characteristics of a closed-end oscillating heat pipe at the normal operating condition, Appl Therm Eng, 23,497–510, 2003.

[11] L. Quan, L. Jia, Experimental study on heat transfer characteristic of plate pulsating heat pipe, the ASME 2009 2nd micro/nanoscale heat & mass transfer international conference, Shanghai, China; 2009.

[12] Q. Cai, C. Chen, J. Asfia, Operating characteristic investigations in pulsating heat pipe, J Heat Transf, 128, 1329–34, 2006.

[13] Q. Cai, R. Chen, C. Chen C, An investigating of evaporation, boiling, and heat transport performance in PHP. New Orleans, Louisiana: ASME International Mechanical Engineering Congress & Exposition; 2002.

[14] L. Xiao, Y. Cao, Recent advances in pulsating heat pipes and its derivatives, J Enhanc Heat Transf, 19,213–231, 2012.

[15] M. Grol, S. Khandekar, State of the art on pulsating heat pipes, the 2nd international conference on microchannels and minichannels, New York, USA; 2004.

[16] J. Qu, H.Y. Wu, Thermal performance of micro pulsating heat pipe, J Chem Ind Eng, 62, 3046–3052, 2011.

[17] W. Qu, C. Qu, J. Feng, Experimental performance of a nanofluid pulsating heat pipe, MicroNano, Kowloon, HongKong; 2008.

[18] H.Y. Lin, S.W. Kang, H.L. Chen, Effect of silver nano-fluid on pulsating heat pipe thermal performance, Appl Therm Eng, 28, 1312–1317, 2008

[19] B. Verma, V.L. Yadav, K.K. Srivastava, Experimental study on thermal performance of pulsating heat pipe with Al2O3–deionized water nanofluid at different orientations, J Enhanc Heat Transf, 20, 153–163, 2013.

[20] Y. Ji, H.B. Ma, H. Chen, Volume fraction effect on heat transfer performance of an oscillating heat pipe, J Thermophys Heat Trans; 27, 111–115, 2013.

[21] M.B. Shafii, A. Faghri, Y.W. Zhang, Thermal modeling of open-looped and looped pulsating heat pipes. J Heat Transf, 123, 1159–1172, 2001.

[22] W. Qu, B. Yang, Performances of flat plate pulsating heat pipes, J Energy Power Eng, 4, 1–8, 2010.

[23] J. Qu, H. Wu, P. Cheng, Experiment study on thermal performance of a silicon-based micro pulsating heat pipe, ASME, Shanghai, China, 2009.

[24] C. Wilson, B. Borgmeyer, R.A. Winholtz, Visual observation of oscillating heat pipes using neutron radiography, J. Thermophys Heat Transf, 2, 366–372, 2008.

[25] B.Y. Tong, T.N. Wong, K.T. Ooi, Closed-loop pulsating heat pipe, Appl Therm Eng, 21, 1845-1962, 2001.

[25] S. Khandekar, M. Groll, An insight into thermal-hydrodynamic coupling in closed loop pulsating heat pipes, Int J. Thermal Sciences, 43, 13-20, 2004.

[26] H.X. Zhi, Q. Wei, Experiment, and theoretical research on an ammonia pulsating heat pipe: New full visualization of flow pattern and operating mechanism study, Int J Heat and Mass Transfer, 106, 149-166, 2017.

[27] M.B. Shafii, A. Faghri, T. Zhang, Thermal modeling of open-looped and looped pulsating heat pipes, J. Heat Transfer, 123, 1159-1172, 2001.

[28] R. Senjaya, T. Inoue, Oscillating heat pipe simulation considering bubble generation Part I: Presentation of the model and effects of a bubble generation, Int Journal of Heat and Mass Transfer, 60, 816-824, 2013.

[29] H. Peng, P.F. Pai, Hongbin Ma, Nonlinear thermomechanical finite-element modeling, analysis and characterization of multi-turn oscillating heat pipes, Int Journal of Heat and Mass Transfer, 69, 424-437, 2014.

[30] I. Nekrashevych, V.S. Nikolayev, Reprint of: Effect of tube heat conduction on the pulsating heat pipe start-up, Applied Thermal Engineering, 126, 1077-1082, 2017.

[31] B. Joohan, L.S. Yong, K.S. Jin, Numerical investigation of effect of film dynamics on fluid motion and thermal performance in pulsating heat pipes, Energy Conversion and Management, 151, 296-310, 2017.

[32] L. Zirong, S. Wang, R. Shirakashi, L.W. Zhang, Simulation of a miniature oscillating heat pipe in bottom heating mode using CFD with unsteady modeling, Int J of Heat and Mass Transfer, 57, 642-656, 2013.

[33] S.M. Pouryoussefi, Y. Zhang, Analysis of chaotic flow in a 2D multi-turn closed-loop pulsating heat pipe, Applied Thermal Engineering, 126, 1069-1076, 2017.

[34] X. Liu, Y. Chen, Fluid flow and heat transfer in flat-plate oscillating heat pipe, Energy and Buildings, 75, 29-42, 2014.

[35] Hyung-Tak Kim, H.K. Park, Kwang Hyun Bang, Heat Dissipation of Sealed LED Light Fixtures Using Pulsating Heat Pipe, Journal of Korean Society of Marine Engineering, 2012, 64-71.

[36] Ansys Fluent Manual 14.5.

# Acknowledgment

First, I would like to express my sincere thanks to my advisor, Professor Kwang-Hyun Bang, for his invaluable advice, guidance throughout my master course. Furthermore, he always gives me the best of mental and material conditions to help me complete my study and research.

I also thank the members of my graduate committee for their guidance and suggestions: Prof. Kweon-Ha Park and Prof. Deog-Hee Doh for their helpful comments and suggestions to complete this dissertation.

I would like to say thank you to all members of Heat Transfer Laboratory, especially Dr. Hyoung-Tak Kim for all his advice, and Vietnamese students in KMOU University for all scientific discussions and helps when I studied in KMOU.

Last but not least I dedicate thankfulness to my family who always encouraged me to achieve whatever goals I set for myself.

Vo Duy Tan

KMOU, Busan, South Korea